PHYSIOLOGY

An evolutionarily conserved olfactory receptor is required for sex differences in blood pressure

Jiaojiao Xu[1], Rira Choi[2], Kunal Gupta[1]†, Helen R. Warren[3,4], Lakshmi Santhanam[2], Jennifer L. Pluznick[1]*

Sex differences in blood pressure are well-established, with premenopausal women having lower blood pressure than men by ~10 millimeters of mercury; however, the underlying mechanisms are not fully understood. We report here that sex differences in blood pressure are absent in olfactory receptor 558 knockout (KO) mice. *Olfr558* localizes to renin-positive cells in the kidney and to vascular smooth muscle cells. Female KOs exhibit increased blood pressure and increased pulse wave velocity. In contrast, male KO mice have decreased renin expression and activity, altered vascular reactivity, and decreased diastolic pressure. A rare *OR51E1* (human ortholog) missense variant has a statistically significant sex interaction effect with diastolic blood pressure, increasing diastolic blood pressure in women but decreasing it in men. In summary, our findings demonstrate an evolutionarily conserved role for OLFR558/OR51E1 to mediate sex differences in blood pressure.

INTRODUCTION

Sex differences in blood pressure are well-established, with premenopausal women having lower blood pressure than men by ~10 mmHg (*1*–*14*). These sex differences are modeled well in C57BL/6 mice, where females have mean arterial pressure (MAP) ~10 mmHg lower than males by telemetry (*1*). However, the blood pressure threshold for treatment of hypertension is identical in men and women (>130/80 for systolic pressure/diastolic pressure), partly because the mechanisms underlying sex differences in blood pressure regulation are only partially understood. Although sex hormones likely contribute to sex differences in blood pressure, they are not fully responsible: Hormone replacement therapy in postmenopausal women does not consistently alter blood pressure (*15*–*17*), and lowered testosterone in aging men is associated with increased risk of cardiovascular diseases (*18*–*20*). Similarly, sex chromosomes may contribute to sex differences in blood pressure but cannot fully explain these differences (*21*).

Olfactory receptors (ORs), the largest family of G protein–coupled receptors (GPCRs), act in the olfactory epithelium (OE) to mediate the sense of smell (*22*). However, ORs are also expressed and play functional roles in non-olfactory tissues such as the kidney, eyes, prostate, and sperm (*23*–*25*). Although there are 1000 murine ORs in the genome, olfactory receptor 558 (OLFR558) is a particularly promising candidate for study. First, *Olfr558* is one of only three mammalian ORs to have been well-conserved by evolution: *Olfr558* has a clear ortholog in all placental mammals, including mice, rats, rabbits, elephants, horses, and five species of primates (*26*–*29*), and the human ortholog [olfactory receptor family 51 subfamily E member 1 (*OR51E1*)] has one of the lowest rates of single-nucleotide polymorphism among human ORs (*30*). Second, *OR51E1* is widely expressed outside the OE in humans [in 13 different tissues (*31*)], and we previously reported that *Olfr558* is expressed in murine kidney (*32*, *33*). Third, most ORs are orphan receptors with no identified ligands; however, we and others have previously identified ligands for OLFR558 and OR51E1, with the strongest ligand being butyrate, one of the major short-chain fatty acids (SCFAs) produced by gut microbiome (*33*–*38*). Thus, we undertook a study to uncover the physiological role of OLFR558 and found that this evolutionarily conserved receptor has a previously unknown role to mediate sex differences in blood pressure.

RESULTS

Olfr558/*OR51E1* is expressed in renin cells and vascular smooth muscle cells

Olfr558 is expressed in the OE (fig. S1) as well as in non-nasal tissues. We previously reported that *Olfr558* is expressed in the kidney (*33*). To date, we have been unable to validate an OLFR558 or OR51E1 antibody; thus, we localized *Olfr558* using RNAScope. In the kidney, *Olfr558* mRNA colocalizes with an antibody for α–smooth muscle actin (α-SMA) in the renal vasculature of *Olfr558* wild-type (*Olfr558* WT) but not *Olfr558* knockout (*Olfr558* KO) kidneys (Fig. 1A). *Olfr558* is also expressed in both afferent and efferent arterioles in the kidney, as identified by costaining for α-SMA protein adjacent to a glomerulus (Fig. 1B) and costaining with a renin antibody (Fig. 1, C and D). Given that α-SMA is expressed in both vascular smooth muscle cells and in fibroblasts (*39*), we double-stained *Olfr558* and *Col1a2* [collagen type 1 alpha 2; fibroblast marker (*40*)] probes in the kidney and found that *Olfr558* is not expressed in *Col1a2*-positive cells (fig. S2, A and B). Thus, these data indicate that *Olfr558* localizes to renal vascular smooth muscle cells.

To determine whether the localization of *Olfr558* to blood vessels occurs beyond the kidney, quantitative polymerase chain reaction (qPCR) was used to identify other organs which express *Olfr558* (Fig. 1E), and subsequently RNAScope was performed on tissues with relatively high expression (table S1 and fig. S3). By qPCR, *Olfr558* is relatively highly expressed in the heart, aorta, brown adipose tissue (BAT), kidney, and skeletal muscle, but exhibits little to no expression in the large intestine, brain, lung, spleen, cecum, or liver.

[1]Department of Physiology, Johns Hopkins University School of Medicine, Baltimore, MD, USA. [2]Department of Anesthesiology and Critical Care Medicine, Johns Hopkins University School of Medicine, Baltimore, MD, USA. [3]Centre of Clinical Pharmacology & Precision Medicine, William Harvey Research Institute, Barts and the London School of Medicine and Dentistry, Queen Mary University of London, London, UK. [4]NIHR Barts Cardiovascular Biomedical Research Centre, Barts and The London School of Medicine and Dentistry, Queen Mary University of London, London, UK.
*Corresponding author. Email: jpluznick@jhmi.edu
†Present address: University of Washington School of Medicine, 1959 NE Pacific St., Seattle, WA 98195, USA.

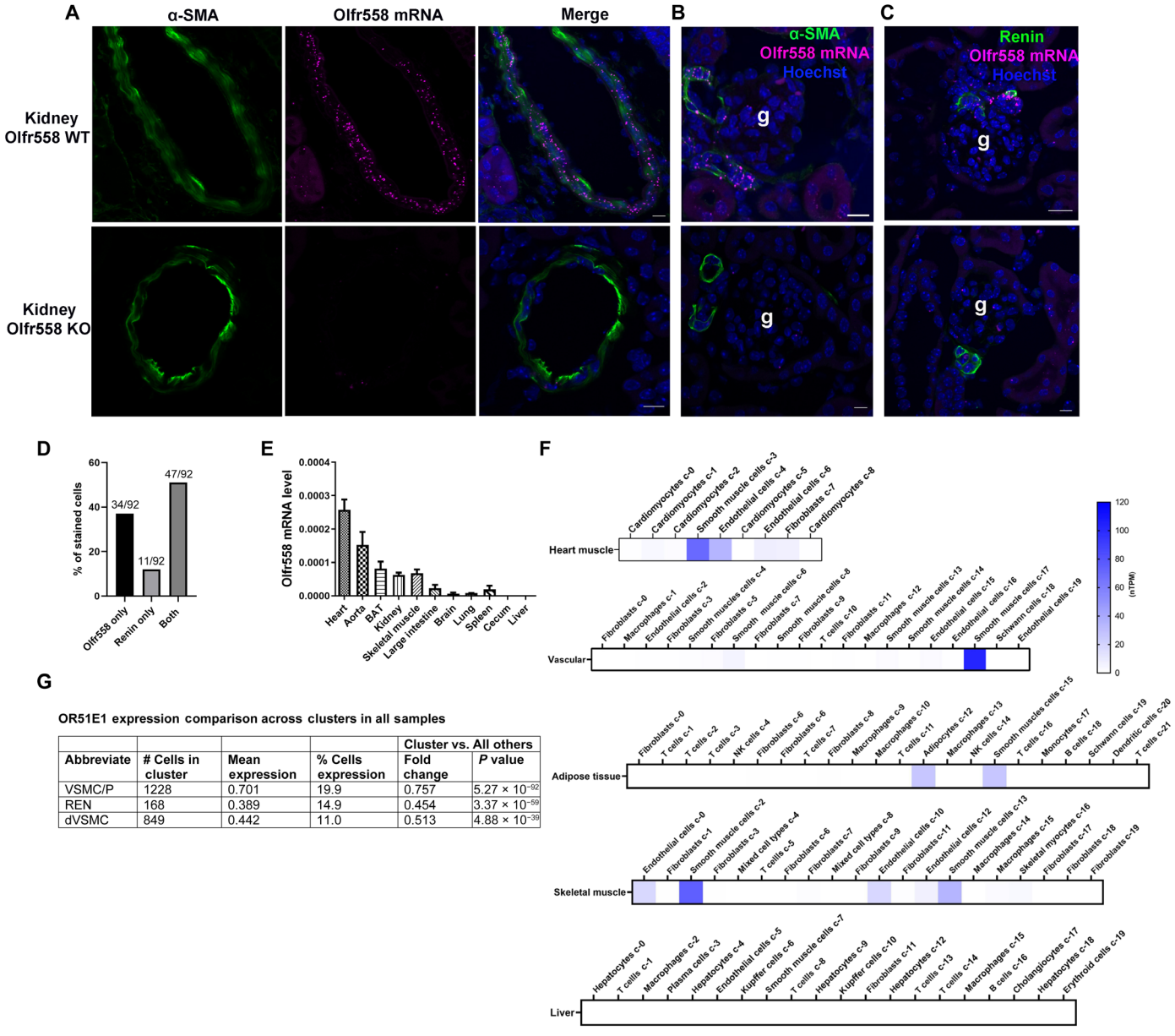

G

OR51E1 expression comparison across clusters in all samples

				Cluster vs. All others	
Abbreviate	**# Cells in cluster**	**Mean expression**	**% Cells expression**	**Fold change**	***P* value**
VSMC/P	1228	0.701	19.9	0.757	5.27×10^{-92}
REN	168	0.389	14.9	0.454	3.37×10^{-59}
dVSMC	849	0.442	11.0	0.513	4.88×10^{-39}

Fig. 1. *Olfr558*/*OR51E1* is expressed in vascular smooth muscle cells. (**A**) Immunostaining (α-SMA; green, blood vessel marker) and RNAScope (*Olfr558* mRNA, purple) demonstrate that *Olfr558* mRNA localizes to vascular smooth muscle cells in *Olfr558* WT kidney (Hoechst nuclear stain, blue, in merge). *Olfr558* mRNA staining is absent in *Olfr558* KO kidney. (**B**) *Olfr558* mRNA is expressed in both afferent and efferent arterioles in *Olfr558* WT but not *Olfr558* KO kidney (Hoechst nuclear stain, blue). (**C**) Costaining with a renin antibody (green) and *Olfr558* RNAScope probe (purple) demonstrates that *Olfr558* is expressed in renin-positive cells in *Olfr558* WT, but not *Olfr558* KO, kidney. Scale bars, 10 μm. One to two dots per cell are occasionally seen outside vascular smooth muscle cells; this likely represents background/genomic DNA (*67*) and not true signal. g, glomerulus. (**D**) RNAScope quantification (renin protein and *Olfr558* mRNA costaining) performed on $n = 92$ cells from $n = 11$ *Olfr558* WT kidney sections from two males. Staining adjacent to the glomerulus was quantified. (**E**) *Olfr558* mRNA expression in a subset of tissues by qPCR. Data normalized to *Gapdh* and averaged from $n = 3$ males and $n = 3$ females. We did not detect any sex differences in *Olfr558* expression. (**F**) Published RNA-seq data from Human Protein Atlas indicates *OR51E1* is primarily expressed in smooth muscle cells in the heart muscle, vascular, adipose, and skeletal muscle. *OR51E1* expression is not detected in the liver. nTMP, normalized transcripts per million. (**G**) *OR51E1* is primarily expressed in vascular smooth muscle and renin cells in kidney. RNA-seq data were downloaded from the Kidney Precision Medicine Project (KPMP). VSMC/P, vascular smooth muscle cell/pericyte; REN, renin-positive juxtaglomerular granular cell; dVSMC, vascular smooth muscle cell (degenerative). KPMP data are from an analysis of 110,346 cells in total comprising 57 kidney cell types.

In the heart, BAT, and skeletal muscle, *Olfr558* localized primarily to vascular smooth muscle cells by RNAScope, although there is rare expression in a minority cell type in skeletal muscle. Using RNAScope and qPCR, we found that *Olfr558* expression is similar between males and females for both kidney and heart (fig. S4); similarly, no sex differences were observed in the qPCR data from Fig. 1E.

We noted that *Olfr558* is typically expressed in some, but not all, vascular smooth muscle cells in a given vessel cross section. The closest "sibling" receptor to *Olfr558*, *Olfr78*, is also expressed in a subset of vascular cells in renal blood vessels (*25*). In olfactory neurons, the expression of ORs is thought to be largely mutually exclusive (one cell–one receptor rule) (*41*). To determine whether *Olfr78*

and *Olfr558* are coexpressed in the kidney and heart, we performed RNAScope for both receptors. In the kidney, the majority of cells express only *Olfr558* (47%) or *Olfr78* (37%), but 16% of cells coexpress both receptors (fig. S5). By contrast, in the heart, 49% of cells coexpress both *Olfr558* and *Olfr78*, but 28% of cells express only *Olfr558* and 23% cells express only *Olfr78* (fig. S5).

We also examined *OR51E1* (human ortholog of *Olfr558*) localization in human tissues using published RNA sequencing (RNA-seq) data. Data (*42*) from the Human Protein Atlas show that *OR51E1* is expressed in human vascular smooth muscle cells in human tissues including the heart, vascular, adipose tissue, and skeletal muscle (Fig. 1F). However, *OR51E1* is not expressed in the liver (Fig. 1F), consistent with our findings in mice (Fig. 1E and table S1). The Human Protein Atlas RNA-seq data for kidney lists only 13 cell types, none of which are vascular smooth muscle cells or juxtaglomerular cells (and none of which express *OR51E1*). Thus, for kidney, we referred to the Kidney Tissue Atlas, which has identified 57 cell types. In human kidney, *OR51E1* is expressed in three cell types: vascular smooth muscle cell/pericyte, renin-positive juxtaglomerular granular cells, and vascular smooth muscle cell (degenerative) (Fig. 1G) (*43*). These findings are consistent with the localization of *Olfr558* expression in mouse tissues.

OLFR558 is required for sex differences in blood pressure

Olfr558 WT and KO mice exhibit no genotypic differences in body weight (fig. S6A), kidney weight/body weight ratio (fig. S6B), heart weight/body weight ratio (fig. S6C), or glomerular filtration rate (GFR) (fig. S6D). Likewise, there are no genotypic differences in blood electrolytes, glucose, blood urea nitrogen, creatinine, or hemoglobin (table S2). On the basis of the localization of *Olfr558* to vascular smooth muscle cells, we hypothesized that *Olfr558* may play a role in blood pressure regulation. To test this hypothesis, we used telemetry to measure 24-hour blood pressure. It is well-established that males have higher blood pressure than premenopausal females by ~10 mmHg in both humans (*2*–*14*) and mice (*1*). In agreement with this, we find that *Olfr558* WT males exhibit significantly higher blood pressure than WT females, including MAP (Fig. 2A), systolic blood pressure (SBP) (Fig. 2B), and diastolic blood pressure (DBP) (Fig. 2C). However, sex differences in blood pressure are absent in *Olfr558* KO (Fig. 2, D to F). *Olfr558* KO females have a significant increase in MAP and DBP in both light (Fig. 2, G and I, and fig. S7, A and C) and dark cycles (Fig. 2, J and L, and Fig. S7, D and F) as compared to WT females. *Olfr558* KO males, as compared to WT males, exhibit a small decrease in DBP without a change in SBP; the drop in DBP is statistically significant during the light cycle (Fig. 2, G to L, and fig. S7, A to F). In addition, "surge BP" [the delta between the lowest blood pressure during the light cycle (6 p.m.) and the highest blood pressure (9 p.m., light off and the start of active period)] is lower in female KO as compared to male KO mice for DBP. In contrast, there is no difference in surge BP between the sexes in WT mice (fig. S8). There are no genotypic differences in heart rate when comparing WT mice to KO mice for either sex (fig. S9, A to D). However, when comparing within the KO genotype, we find that female KOs have higher heart rate than male KOs. No genotypic or sex differences are seen in pulse pressure (fig. S9, E to H). We also note that KO females are more active than KO males. In addition, in females, KOs are more active than WTs during the dark but not the light cycle (fig. S9, I to L). Notably, other sex differences (not related to blood pressure) are intact in *Olfr558* KO: for example, KO males weigh more than KO females (fig. S6A), and KO males and females are fertile. Given the lack of sex differences in blood pressure in KO mice, we expanded our localization of *Olfr558* to include testes and ovaries: In testes, *Olfr558* not only is expressed primarily in blood vessels but is also seen in a minority cell type (fig. S10). In ovaries, *Olfr558* is solely expressed in blood vessels (fig. S11).

OLFR558 modulates renin in males

Given the localization of *Olfr558* to renin-expressing cells in the renal afferent arteriole, we examined a potential role for *OLFR558* to regulate renin. Using qPCR, we find that *Olfr558* mRNA is absent in KO kidneys (Fig. 3, A and F), as expected. In KO female versus WT female kidneys, we find no differences in renin mRNA (Fig. 3B), no differences in the percentage of renin positive to total glomeruli (Fig. 3, C and D), and no differences in plasma renin activity (PRA) (Fig. 3E). In KO male versus WT male kidneys, we find a significant decrease in renin mRNA (Fig. 3G), a reduction in the percentage of renin positive to total glomeruli (Fig. 3H), and decreased PRA on two different diets (0.2% NaCl, Fig. 3I; 0.49% NaCl, Fig. 3J) in KOs. Notably, renin mRNA expression exhibits no difference between *Olfr558* WT and KO males in the heart (fig. S12). These data suggest that OLFR558 acts to support renin levels in WT males, and thus changes in renin may contribute to the lower blood pressure in male KOs.

To determine whether the changes in male KOs are due to a decreased number of renin cells, we costained renin and α-SMA in male *Olfr558* WT and KO kidneys (Fig. 4A) and quantified the number of cells that costained for both markers or for either one alone [as done previously (*44*)]. We find a decreased number of cells staining for "renin only" in male KO mice and, to a lesser extent, a decreased number of cells labeling for both α-SMA and renin (Fig. 4B). Similarly, qPCR for the renin cell marker *Akr1b7* revealed a decrease in renal *Akr1b7* expression in male but not female KO (Fig. 4, C and D).

OLFR558 modulates vasoreactivity in males

Given the localization of *Olfr558* to vascular smooth muscle cells in a variety of vascular beds, we examined a role for OLFR558 to regulate vasoreactivity in aortic rings and mesenteric arteries. We first confirmed that *Olfr558* is expressed in aortic rings and mesenteric arteries by reverse transcription PCR (RT-PCR) (fig. S13). Ex vivo vascular reactivity studies show that *Olfr558* KO aortic rings from females exhibit higher maximal contractility induced by potassium chloride (KCl) as compared to WT. Similar responses to phenylephrine (PE), acetylcholine (ACh), and sodium nitroprusside (SNP) (fig. S14, A to D) suggest no impairments in vascular smooth muscle or endothelial function in female KO. In males, KO aortic rings exhibit less constriction to PE (fig. S14F). In contrast, there were no genotypic differences in males to the constriction to KCl (fig. S14E) or relaxation to ACh (fig. S14G) or SNP (fig. S14H).

Olfr558 KO mesenteric arteries from females demonstrate similar constriction to KCl and PE and similar relaxation to ACh and SNP (Fig. 5, A to D). In males, there are no genotypic differences in the constriction to KCl and PE or in the relaxation to ACh (Fig. 5, E to G). However, *Olfr558* KO mesentery from males exhibit increased relaxation to SNP, which could contribute to the decreased blood pressure in males (Fig. 5H).

OLFR558 modulates arterial stiffness in females

Data from the studies described above imply that the decreased DBP in the males may be driven by decreased renin and/or an exaggerated relaxation to SNP in the mesentery. However, the only genotypic

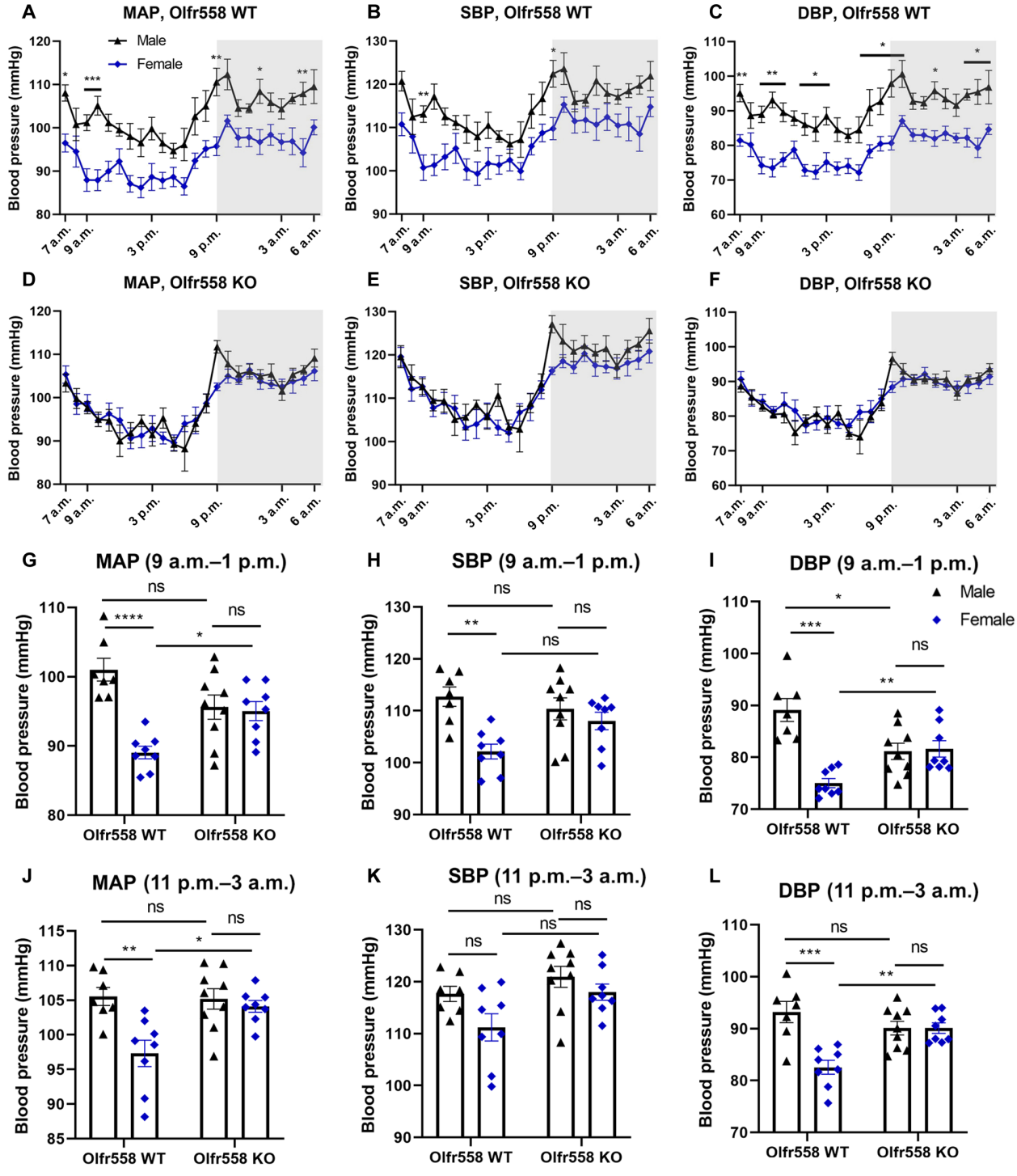

Fig. 2. *OLFR558* regulation of blood pressure is sex specific. Blood pressure was measured by telemetry. *Olfr558* WT mice exhibit previously reported sex differences in (**A**) MAP, (**B**) SBP, and (**C**) DBP. These differences are absent in *Olfr558* KO (**D** to **F**) due to increased blood pressure in females, along with decreased male DBP. Gray areas depict the active (dark, 9 p.m.to 7 a.m.) phase, and white areas depict the resting (light, 7 a.m. to 9 p.m.) phase. Averaged data from the light cycle (9 a.m. to 1 p.m.) are shown in (**G** to **I**), and averaged data from the dark cycle (11 p.m. to 3 a.m.) are shown in (**J** to **L**). Male WT: $n = 7$, male KO: $n = 9$. Female WT and KO: $n = 8$. $^{*}P < 0.05$, $^{**}P < 0.01$, $^{***}P < 0.001$, and $^{****}P < 0.0001$ by phenotype (*Olfr558* WT versus KO) and sex (male versus female) using two-way analysis of variance (ANOVA). ns, nonsignificant.

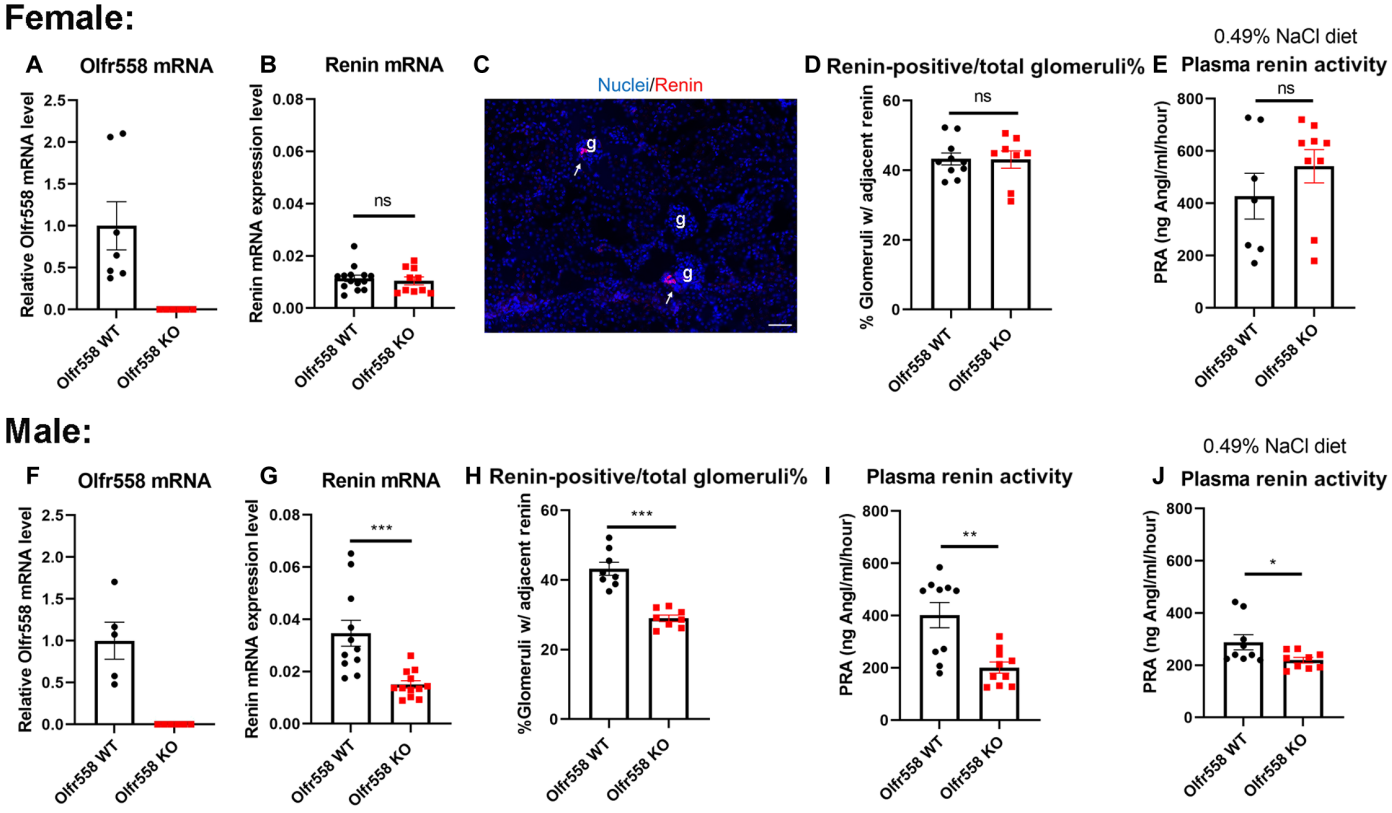

Fig. 3. *Olfr558* modulates renin in males. (**A** and **F**) *Olfr558* mRNA is absent in kidneys of *Olfr558* KO. *Renin* mRNA levels in the kidney are not altered in females (**B**) but are decreased in KO males (**G**). Renin antibody staining (red, white arrow) is observed in glomerulus (**C**). Scale bar, 50 μm. (**D** and **H**) Ratio of renin-positive/total glomeruli is reduced in male KOs but not females. PRA is decreased in male KOs on standard chow (**I**) and 0.49% NaCl diet (**J**) but is not altered in KO females (**E**). Notably, (A) to (D) and (F) to (I) mice were treated with the same diet as for the telemetry data. The relative mRNA expression is presented normalized to its *Gapdh* or *Gapdh* and WT of the same sex. $*P < 0.05$, $**P < 0.01$, and $***P < 0.001$. ns, nonsignificant by *t* test.

difference in females was KCl constriction in the aorta. Thus, to better understand the female phenotype, we evaluated the mechanical properties of female aortas ex vivo and measured arterial stiffness in females in vivo. The tensile properties are similar between *Olfr558* WT and *Olfr558* KO in both intact and decellularized aortic rings from 10-week-old female mice (Fig. 6A). Likewise, there are no differences in the wall thickness and diameter of aortic rings from 10-week-old *Olfr558* WT and KO females (Fig. 6, B and C). However, pulse wave velocity (PWV) is significantly increased in 10-week-old *Olfr558* KO females as compared to WT (Fig. 6D), implying that increased vascular stiffness may contribute to the female KO phenotype. Together, these data suggest that the in vivo smooth muscle tone is responsible for the higher PWV noted in KO females, but that OLFR558 does not contribute significantly to passive mechanical stiffness of the matrix.

Gut microbiome is similar in *Olfr558* WT and KO mice

Butyrate, an SCFA produced by gut microbes, is the ligand that yields the strongest activation of both OLFR558 and OR51E1 (*33, 34*). In addition, several other ligands for OLFR558/OR51E1 are also produced by gut microbiota, including isovaleric acid (IVA) and valeric acid (VA) (*33, 34*). Thus, baseline differences in the gut microbiome of WT versus KO mice could contribute to the phenotype. To interrogate this possibility, we analyzed 16*S* ribosomal RNA (rRNA) from fecal DNA from *Olfr558* WT and KO (females and males). The major phyla show no differences between WT and KO (fig. S15), indicating that WT and KO have similar microbes, and thus differences in the gut microbiome are an unlikely explanation for the KO phenotype.

Human variants in OR51E1 alter blood pressure in men and women

The human ortholog of OLFR558 is OR51E1. An *OR51E1* variant was previously identified by Evangelou *et al.* (*45*) as significantly associated with DBP (rs17224476): In the total genome-wide association study (GWAS) meta-analysis ($N \sim 750{,}000$), each copy of the minor allele A increased DBP by ~0.16 mmHg ($P = 7.37\times 10^{-9}$) according to an additive allelic association model. However, this previous GWAS did not examine sex-specific effects. So, here, we performed sex- and age-stratified analyses on *OR51E1* variants using U.K. Biobank (UKB) data. Our analysis focused on the lead, common, missense variant (rs17224476) from the Evaneglou *et al.* study and also on a rare missense variant (rs202113356), which we have previously studied in vitro (*34*). Within UKB data, the common variant (rs17224476) has minor allele frequency (MAF) = 11.1%, and the rare variant (rs202113356) has MAF = 0.025%. Although these two variants are located very close together on the genome, only 434 base pair apart, they are independent, uncorrelated variants, and calculated within UKB to not be in linkage-disequilibrium ($r^2 \sim 1 \times 10^{-5}$, very close to 0).

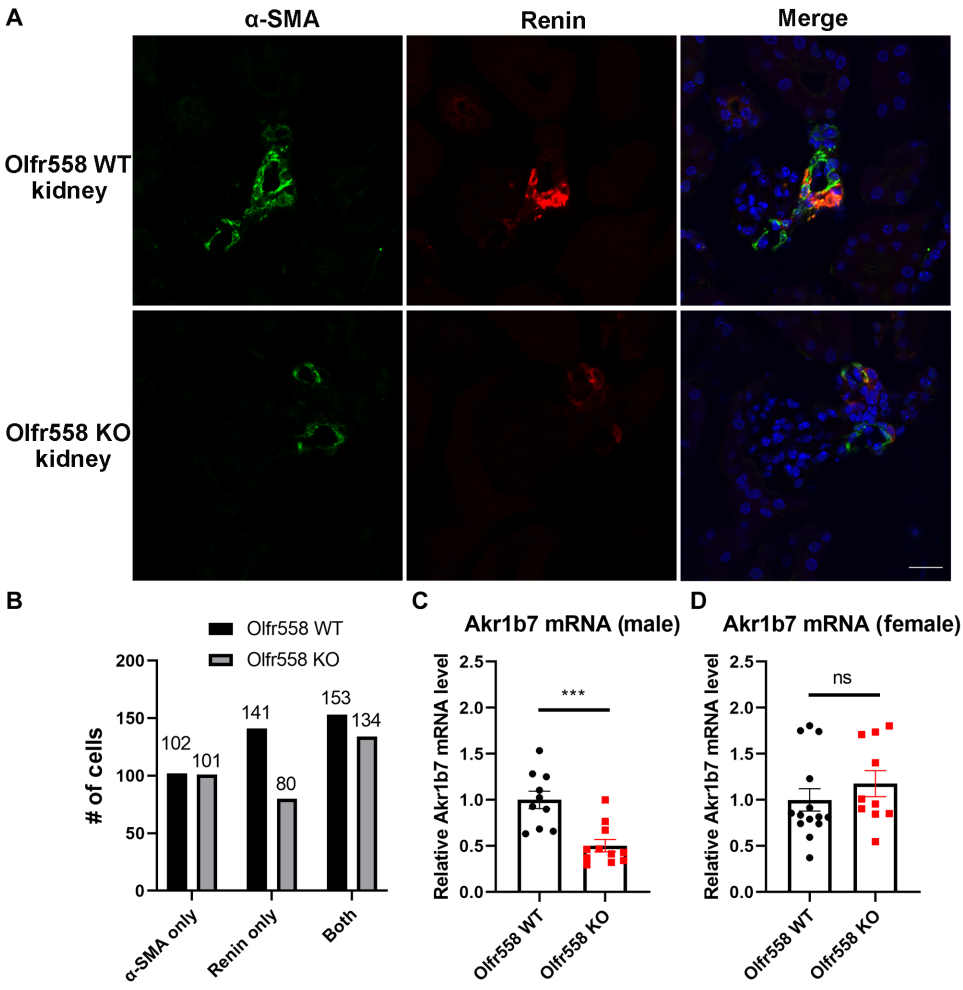

Fig. 4. Renin-expressing cells are decreased in male *Olfr558* KOs. Costaining of α-SMA (green) and renin (red) was examined from male WT and KO kidneys (**A**). Juxtaglomerular apparatus (JGA)-associated cells were counted as α-SMA only, renin only, or α-SMA and renin (both) expression; this quantification indicates that the number of renin-expressing cells is decreased in male KO (**B**). $n = 4$ WT and KO. *Akr1b7* (renin cell marker) mRNA expression is reduced in KO males (**C**) but not females (**D**). Scale bar: 20 μm. ***$P < 0.001$.

We confirm the previously published association of the lead variant in the total sample, with the association for DBP still being highly significant in the UKB data alone ($P = 4.27 \times 10^{-5}$; $N = 423{,}655$). This lead variant is significantly associated with DBP within each of the separate men and women subgroups with the minor allele A increasing DBP similarly in both men and women, showing no significant sex-interaction ($P = 0.76$) (Fig. 7, A to C and tables S3 and S4). This variant is also significant ($P < 0.05$) for females <50, females >50, and males >50 within the stratified analyses (Fig. 7A) and with no significant evidence of any age-interaction effect (Fig. 7C). So, for this common variant, there is sufficient statistical power to clearly demonstrate the significant association of *OR51E1* with DBP overall, showing across all subgroup analyses, that the minor allele A of this variant increases DBP. These data therefore confirm and expand the role of this OR in blood pressure regulation and imply that common frequency variants in this receptor affect blood pressure equally in men and women.

We also examined a rare variant, which is also localized to an exon and is primarily seen in South Asia. We previously published that this rare variant alters OR51E1 function in vitro (rs202113356) (*34*). The highlighting result from our UKB analyses is that this rare variant has a significant sex-interaction result ($P = 0.015$), showing sex-specific effects, with opposite directions of effect in men versus women (Fig. 7, D to F, and table S4). The association is nominally significant ($P = 0.053$) within females, with the minor allele A increasing DBP by +6.28 mmHg for female carriers (AG) versus female non-carriers (GG). In contrast, within males, the effect estimate (−4.77 mmHg) indicates that the rare variant decreases DBP in men, and the association result is not significant ($P = 0.149$), which could either be due to a lack of association in males completely relating to the sex-specific nature of the variant or simply due to lack of statistical power for analysis of the rare variant (Fig. 7D). Furthermore, from the age-stratified analyses within females, there is a stronger association in younger females with a more significant result despite a lower sample size ($P = 0.0501$; $N = 57{,}464$) in women <50 years compared to in women >50 years ($P = 0.29$; $N = 171{,}067$) and also a much larger effect size (+13.44 mmHg in women <50 versus +3.89 mmHg in women >50) (Fig. 7D), as can also be seen by the steeper gradient of the effect slope (Fig. 7F), although there is no significant age-interaction effect ($P = 0.26$), likely due to a lack of statistical power

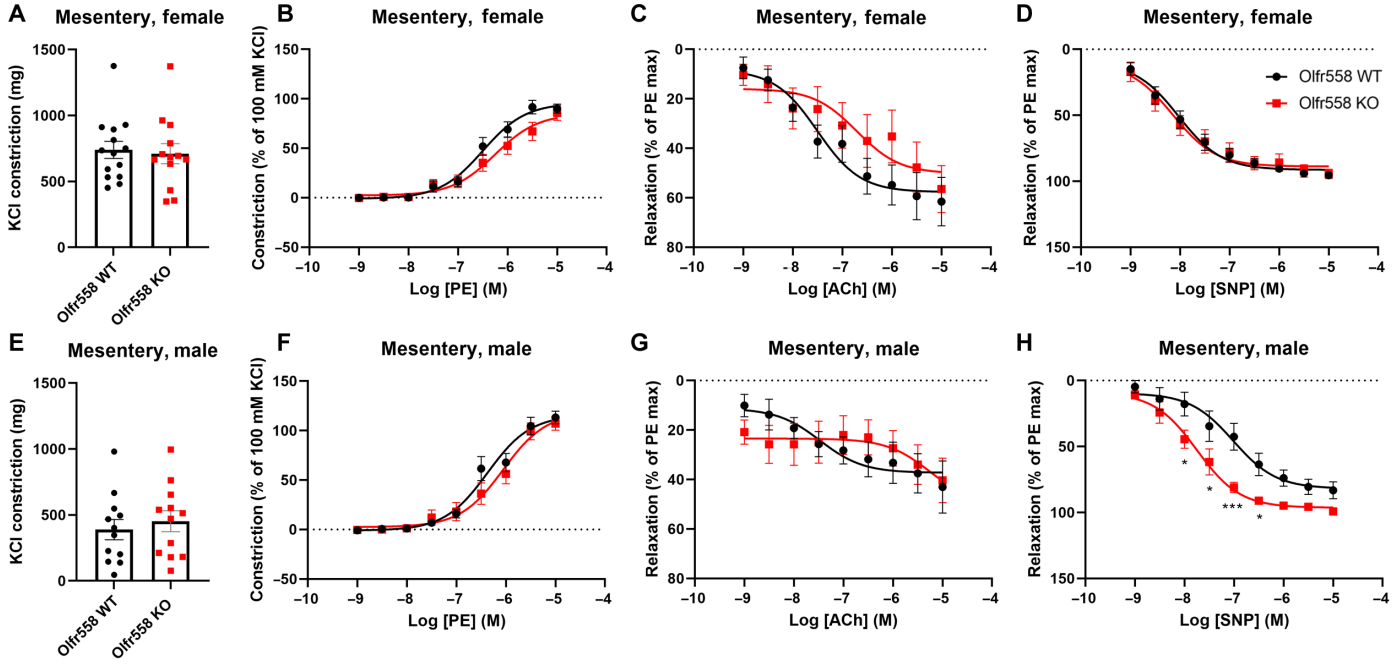

Fig. 5. Mesentery vasoreactivity in *Olfr558* WT and KO females and males. No genotypic differences were observed in mesentery constriction to 100 mM KCl (**A** and **E**), mesentery constriction to PE (**B** and **F**), or mesentery relaxation to ACh (endothelium dependent) (**C** and **G**). However, endothelium-independent vasorelaxation in response to SNP (endothelium independent) was enhanced in KO males (**H**) but not females (**D**). PE responses are normalized to the KCl response, and ACh and SNP responses are normalized to the maximum PE response. $n = 8$ to 14 Mesenteric arteries from $n = 7$ *Olfr558* WT and KO females. $^{**}P < 0.01$ and $^{***}P < 0.001$ by *t* test for (A) and (E) and two-way ANOVA for (B) to (D) and (F) to (H).

for detecting a higher-order interaction effect within a smaller stratified analysis sample for a rare variant. Acknowledging that we always expect less statistical power for such a rare variant, the significant sex-interaction results for this rare variant (Fig. 7E) is therefore a very clear conclusion, indicating that this variant has a strong, differential effect on DBP with opposing effects in men versus women.

OR activity is reduced in cells transfected with the OR51E1 variants

Given these findings, we further examined both variants using in vitro studies to determine whether they have altered responses to known ligands. The common (rs17224476) variant results in a missense change (S10N). (Notably, the "S" residue is conserved in numerous species, including humans, mouse, and rat.) We find that OR51E1 S10N shows similar cell surface trafficking (fig. S17) and total protein expression (fig. S16) as WT OR51E1. However, in the absence of Golf (olfactory G protein), butyrate-induced cyclic adenosine 3′,5′-monophosphate (cAMP) production is significantly and dose dependently attenuated in OR51E1 S10N–transfected cells (Fig. 8, A and B). Results with other ligands [which we have previously identified for the WT receptor (*33*)] did not reach statistical significance in the absence of Golf (Fig. 8C). When cotransfected with Golf, the reduction in OR51E1 S10N signaling is significant for all ligands tested (Fig. 8, B and D).

The rare variant (rs202113356) also results in a missense change (A156T). For OR51E1 A156T, we recently published that OR51E1 A156T exhibits less cell surface but similar total protein expression as OR51E1 (*34*). We also reported that butyrate activation is significantly and dose dependently reduced in OR51E1 A156T–and/or Golf-transfected cells (*34*). Here, we further evaluated the response of OR51E1 A156T to other ligands and found that cAMP production is also attenuated in OR51E1 A156T–transfected cells for all ligands tested (Fig. 8, E and F).

DISCUSSION

We report here that OLFR558 is required for sex differences in blood pressure. *Olfr558* localizes to vascular smooth muscle cells in a subset of non-nasal tissues including the kidney, heart, BAT, skeletal muscle, testes, and ovaries but is absent from other tissues (e.g., the liver). In the kidney, *Olfr558* is expressed in both afferent and efferent arterioles, including renin-positive cells. Functional studies using *Olfr558* WT and KO mice demonstrate that the sex difference in blood pressure is intact in *Olfr558* WT but absent in *Olfr558* KO mice, suggesting that OLFR558 is required for sex differences in blood pressure. The loss of sex differences in the KO appears primarily driven by increased blood pressure in females, with a more minor contribution of decreased blood pressure in males. The increased blood pressure in KO females may be driven by increased vascular stiffness, as indicated by the elevated PWV. Lowered DBP in the males may be driven by decreased plasma renin and an exaggerated relaxation to SNP in the mesentery. The directionality of the changes in renin, vascular reactivity, and arterial stiffness indicates that these changes may contribute to the change in blood pressure (compensatory changes would be expected to be in the opposite direction). In humans, *OR51E1* has been identified as a locus that is associated with significant changes in DBP. We find that a rare *OR51E1* variant induces changes in DBP, which match both the direction (increased in females and decreased in males) and the magnitude seen in KO mice of each sex. Together, these data imply that

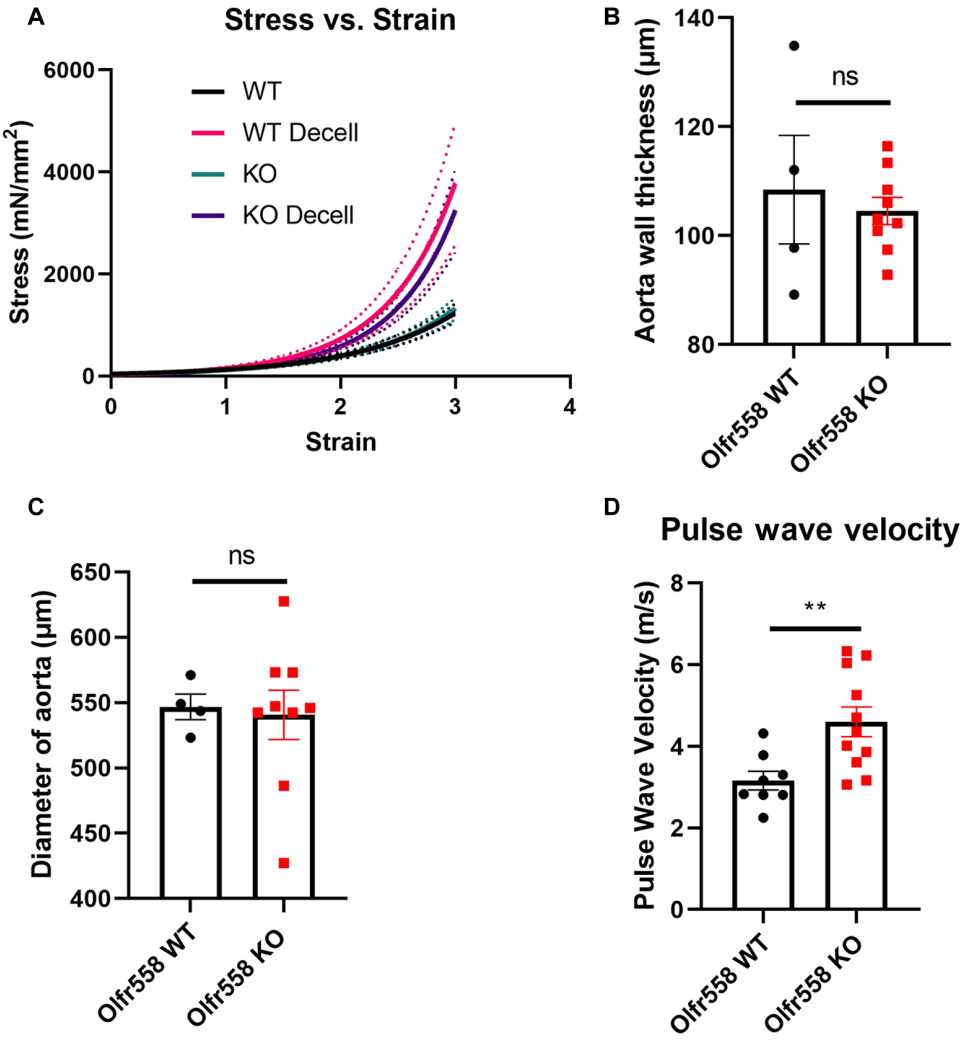

Fig. 6. Increased arterial stiffness in *Olfr558* KO females. (**A**) Tensile testing of intact and decellularized thoracic aortic rings from *Olfr558* WT and KO females did not reveal genotypic differences. Likewise, there were no genotypic differences in wall thickness (**B**) or aortic diameter (**C**). (A to C: $n = 4$ for WT, $n = 9$ for KO). (**D**) However, PWV, an in vivo measure of arterial stiffness, is higher in *Olfr558* KO females. $n = 8$ for WT, $n = 11$ for KO. $^{**}P < 0.01$ by *t* test.

this evolutionarily conserved OR is required for sex differences in blood pressure through a mechanism that involves modulation of both renin and in vivo smooth muscle tone.

OLFR558 and OR51E1 localization

Our studies demonstrate that OLFR558/OR51E1 is broadly expressed in non-nasal tissues, where it localizes to blood vessels in both mice and humans. Our findings are supported by a report that *Olfr558* is expressed in the blood vessels of the eye (*24*), a report that the rat ortholog of *Olfr558* (Olr63) is associated with glomeruli (*46*), and a study (*47*) that used microarray to identify genes that confer the identity of the renin cell. Intriguingly, this latter study also reported that *Olfr558* is up-regulated in response to captopril treatment, implying that *Olfr558* expression is regulated in response to changes in blood pressure. It has also been reported that *Olfr558* is highly and selectively expressed in the carotid body (*48*) and that *Olfr558* localizes to vascular smooth muscle cells of carotid body blood vessels using an *Olfr558* lacZ knock-in reporter allele (*48*), consistent with our findings. *Olfr558* is expressed in vascular smooth muscle cells but not endothelial cells or fibroblasts by RNAScope; this is in agreement with published single-cell RNA-seq (scRNA-seq) data showing that OR51E1 is expressed in vascular smooth muscle but not endothelial cells or fibroblasts in human vascular tissue (and most other tissues) (*42, 43*). Although these scRNA-seq databases do show *OR51E1* expression, we should note that ORs are sometimes absent from scRNA-seq databases. This is likely due to the fact that ORs are the largest gene family in the genome (~1000 genes in mice and ~350 genes in humans), and thus short sequencing reads for ORs may be discarded if they match multiple genes. In addition, GPCRs (including ORs) have relatively low levels of expression, which may also be "missed" by RNA-seq depending upon read depth.

Notably, we did not observe any sex differences in expression of *Olfr558*. Although there is a previous report that OR51E1 is expressed in renal epithelial cells (both in the HK-2 human proximal tubule cell line and in human kidney) (*38*), we did not observe localization to renal tubular epithelial cells by RNAScope; similarly, *Olfr558* has previously been reported to expressed in enterochromaffin cells, which we did not investigate in this study (*49*).

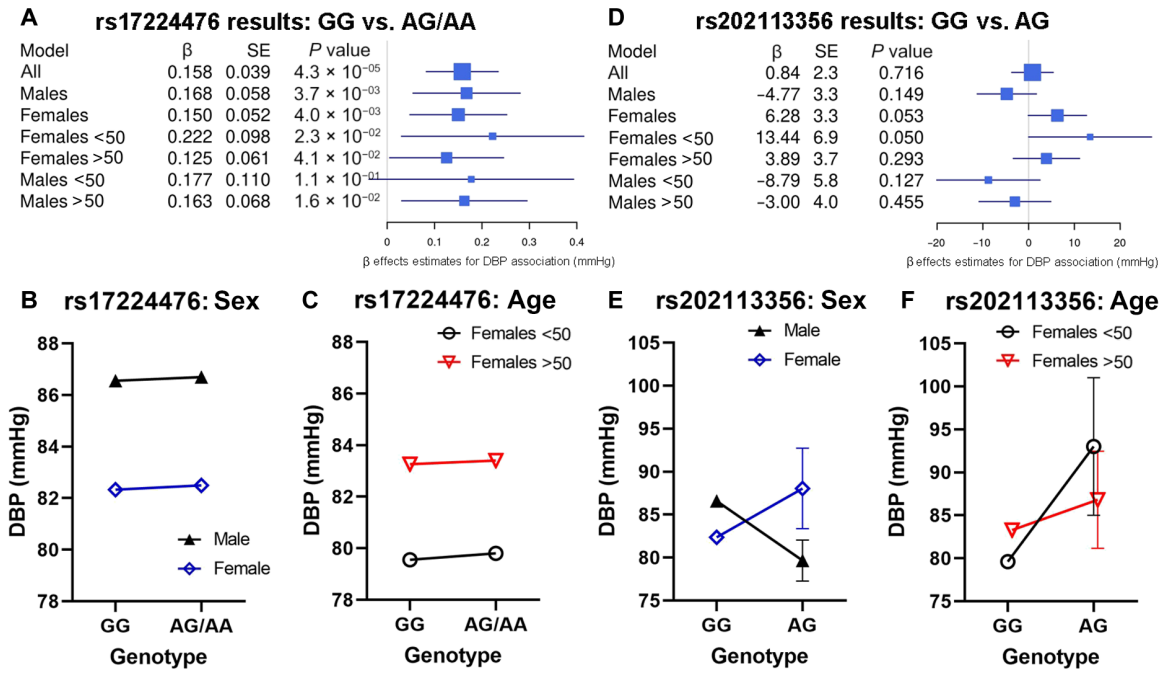

Fig. 7. *OR51E1* variants and blood pressure. (**A** to **C**) Lead variant (rs17224476); (**D** to **F**) Rare variant (rs202113356). (A) and (D) Forest plots illustrating all association results for different subgroup models for each variant. A positive β value for the linear regression effect estimate indicates that the minor allele A of the variant increases DBP, whereas a negative β value indicates that the minor allele A of the variant decreases DBP. $P < 0.05$ is declared as significant. (B) and (E) Sex-stratified analyses comparing the mean DBP in noncarriers (GG) versus carriers of the minor allele (AG/AA) separately in males versus females. (C) and (F) Age-stratified analyses comparing the mean DBP in noncarriers (GG) versus carriers of the minor allele (AG/AA) separately in younger women <50 years versus older women >50 years. In these stratified analysis plots, the mean DBP values within each subgroup are plotted together with the interval limits for the SEM bars. The lead *OR51E1* variant (rs17224476) is significantly associated with DBP overall and within sex- and age-stratified analyses [(A) to (C)]. The minor allele A of this variant increases DBP within all individuals, without any sex (B) or age (C) interactions. The rare *OR51E1* variant (rs202113356) has a significant sex-interaction effect ($P = 0.0148$) (E), with sex-specific opposing effects on DBP in males versus females [(D) to (F)]. The rare variant decreases DBP in men but increases DBP in women (D).

Sex differences in blood pressure

Sex differences in blood pressure in normotensive subjects are well-documented in both animal models (*1*) and humans (*1*–*14*). In humans, 24-hour ambulatory blood pressure measurements show that men have higher SBP (~10 mmHg) than women from the ages of 20 to 70; this difference is absent in those above the age of 70 (*6*). Furthermore, a study of 27,542 participants demonstrated that not only do women have lower blood pressure than men, but also women incur increased risk for cardiovascular disease at lower blood pressures than men (*10*): For example, the stoke risk for women with SBP from 120 to 129 mmHg is comparable to the risk for men with SBP from 140 to 149 (*10*), highlighting the clinical relevance of these sex differences. The sex differences in blood pressure seen in humans are also observed in mice, where the MAP of males is ~10 mmHg higher than that of females by telemetry (*1*). This differences persists through 12 months of age but is absent by 18 months of age due to an increase in female blood pressure (*1*). Consistent with previous report, we find that *Olfr558* WT males have blood pressure that is ~10 mmHg higher than females (Fig. 2). However, this blood pressure difference is absent in *Olfr558* KO mice (Fig. 2), indicating that Olfr558 is required for sex differences in blood pressure. We also noted that DBP exhibits no significant difference between male WT and KO mice during the dark cycle; this could be due to an increase in activity of the mice during the dark cycle leading to a greater DBP variability. Notably, activity data from the telemeters indicates that KO females are more active than KO males, and KO females are more active than WT females during the dark but not the light cycle. Given that the difference in blood pressure (both MAP and DBP) between WT and KO females persists during both the dark and light cycles, activity alone is unlikely to explain the blood pressure phenotype; however, this factor could certainly play a contributory role. Notably, differences in sodium intake could also contribute to differences in blood pressure and were not examined in this study.

From our UKB analyses (Fig. 7E), although baseline blood pressure is higher in males, the sex-specific opposing effects of the rare variant (rs202113356) lead to male minor allele carriers having lower mean DBP than noncarrier females; and vice versa, that female minor allele carriers have higher mean DBP than noncarrier males, demonstrating how the effect of the genetic variant completely counterbalances and switches the normal underlying blood pressure levels in men and women.

Renin

Sex differences in renin expression have previously been reported. For example, the renal renin concentration in adult females is lower than that of males in both Wistar and Sprague-Dawley rats (*50*). Similarly, we find that *Olfr558* WT female kidneys have less renin mRNA than male kidneys ($P < 0.01$ by *t* test; Fig. 3, B versus G); this sex difference is muted in KO mice. In our hands, PRA exhibited no differences between WT males and females (Fig. 3); this is in agreement with a previous study showing that PRA is similar in normotensive men and women (*51*) as well as in Lewis rats (*52*).

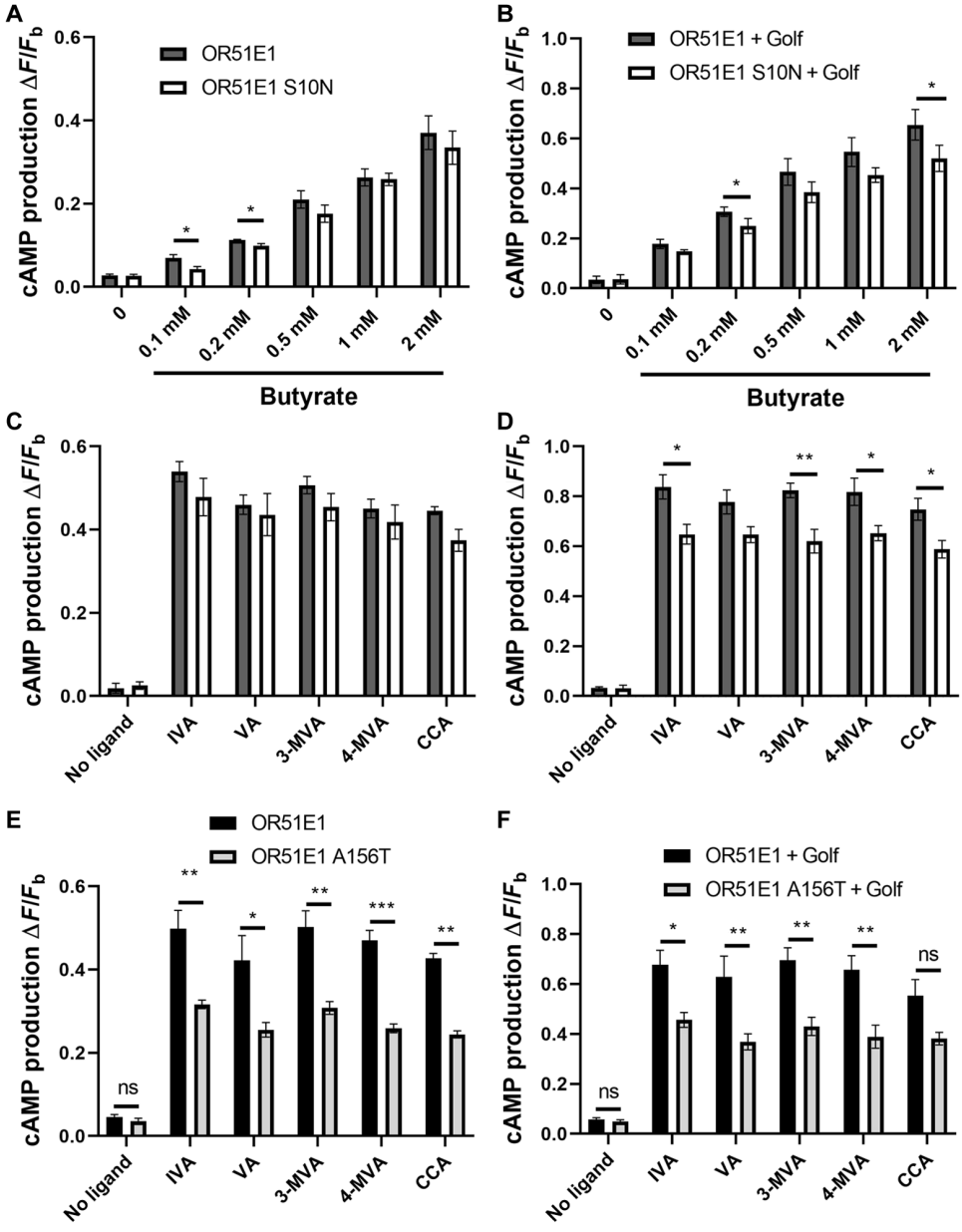

Fig. 8. OR51E1 mutants have reduced activity as compared to WT OR51E1. (**A** and **B**) Butyrate-induced cAMP production is significantly attenuated in OR51E1 S10N–transfected cells with or without Golf cotransfection. For other ligands, the difference between WT and S10N is significant with but not without Golf (**C** and **D**). (**E** and **F**) Ligand-induced cAMP production is reduced in OR51E1 A156T–transfected cells with or without Golf cotransfection. $\Delta F/F_b = (F_{ligand} - F_{baseline})/F_{baseline}$. IVA, isovaleric acid; VA, valeric acid; 3-MVA, 3-methylvaleric acid; 4-MVA, 4-methylvaleric acid; CCA, cyclobutane-carboxylic acid. Ligands in (C) to (F) were tested at 1 mM. $^*P < 0.05$ and $^{**}P < 0.01$ OR51E1 (+Golf) versus OR51E1 S10N or OR51E1 A56T (+Golf) by ANOVA.

As for genotypic differences, we find that male KO (versus male WT) have decreased renin mRNA, decreased glomeruli-associated renin positive cells, and decreased PRA (Figs. 3 and 4). Moreover, male KO exhibit a decreased number of cells staining for renin only and for both α-SMA and renin, suggesting that decreased renin in male KO is primarily driven by a decreased number of renin-expressing cells (as opposed to a change in protein amount per cell), possibly reflecting a change in renin cell recruitment (*53*). Notably, low renin paired with lowered blood pressure implies that the low renin is a contributing factor to the blood pressure change, as otherwise one would expect renin to be elevated when blood pressure is lowered. However, if lowered renin were fully responsible for the male blood pressure phenotype, diastolic and systolic pressure should be altered equally. Instead, KO males exhibit isolated lower diastolic BP. Furthermore, renin is not altered in WT versus KO females (Fig. 3). Therefore, Olfr558-induced sex differences in blood pressure cannot be explained by renin alone. In addition, a microarray study indicates that *Olfr558* expression may decrease through renal development (*47*), indicating the importance of better understanding if OLFR558 is involved in renal development.

Vascular tone

We find that *Olfr558* WT males and females exhibit similar responses to PE and ACh in both aortic rings and mesenteric arteries ex vivo (Fig. 5). This is consistent with a previous report that mesenteric arteries demonstrate similar relaxation to ACh in female and male rats and were unaffected by ovariectomy (*54*), but contradicts reports that aortic rings show more constriction to PE in male versus female rats (*55, 56*). It has also been reported that vascular constriction is significantly enhanced in ovariectomized versus intact female rats (with no difference between castrated and intact male rats), suggesting that the sex differences in vascular tone are likely related to sex hormones (*57*). Notably, the maximum contraction to KCl in WT mesenteric arteries is higher in females versus males (Fig. 5).

As for genotypic differences, male KOs exhibit decreased constriction to PE in the aorta and exaggerated relaxation to SNP in the mesentery as compared to WT males. However, ex vivo studies in females found no differences in the response to PE, ACh, or SNP in WT versus KO. Although KO females do have an increased response to KCl in the aorta, this alone seems unlikely to explain the blood pressure phenotype. However, female KOs manifest increased PWV in vivo, indicating stiffer blood vessels that could contribute to the increased blood pressure in KO females. The fact that the female KO vessels appeared normal ex vivo but were stiffer in vivo implies that there may be a circulating factors or hormones required to manifest the phenotype. Although we acknowledge that these studies have used whole-animal *Olfr558* KOs, the localization of *Olfr558* is quite specific to vascular smooth muscle and renin-specific cells (Fig. 1 and figs. S2 to S5), and we see changes in vascular reactivity ex vivo (Fig. 5). Thus, we conclude that smooth muscle cells (together with renin cells) drive the blood pressure phenotype. However, future studies using renin-specific or smooth muscle cell–specific KO mice models will allow us to dissect the precise contribution of renin versus smooth muscle cells in mediating sex differences in blood pressure. Similarly, the whole-animal KO does not allow us to assay a potential role of developmental processes; this will be another key area to explore in future studies.

Human genetic analysis

In support of a role for this evolutionarily conserved OR in blood pressure regulation, *OR51E1* was previously identified as a locus associated with DBP (*45*). We report here that a (relatively) common *OR51E1* variant (rs17224476; MAF = 11.1%) is associated with increased DBP and affects blood pressure similarly in both men and women, whereas a rare *OR51E1* variant (rs202113356; MAF = 0.025%) effects blood pressure in the opposite direction in men as opposed to women. Notably, both the magnitude and the direction of the change in blood pressure for the rare variant is remarkably similar to the changes seen in male and female *Olfr558* KO. It is also intriguing that the rare variant seems to have a stronger effect to increase blood pressure in women <50 versus women >50. It is imperative to note that due to the rarity of this variant, the number of patients with this variant is quite small and thus we must interpret our conclusions appropriately according to the reduced statistical power. However, the presence of a variant in humans that differentially alters blood pressure by sex is supportive of the idea that our findings in mice are relevant to other species, including humans, especially when we observe such consistency and similarity in the effect estimates from our analyses in both humans and mice.

OLFR558/OR51E1 trafficking and ligands

To explore how these two OR51E1 variants may alter the cell biology of OR51E1 signaling, we carried out in vitro studies. We previously published that the surface expression of the rare variant is reduced as compared to WT (*34*); however, we find here that the common variant does not alter surface expression. We previously reported that butyrate is the best ligand for OLFR558/OR51E1 and that other ligands including IVA, VA, 3-methylvaleric acid (3-MVA), 4-methylvaleric acid (4-MVA), and cyclobutane-carboxylic acid (CCA) also activate OLFR558 and OR51E1 (*33*). In this study, we find that the activity of both the common and rare variants is reduced in vitro compared to WT OR51E1. Given that both variants reduce OR51E1 activity, yet the effects of the variants in vivo are different in each sex, it seems likely factors are missing from our in vitro system which prevent full recapitulation of OR51E1 biology. These factors may include sex chromosomal effects (HEK293T are XX), the absence of gonadal hormones, or downstream signaling partners. Notably, in our in vivo studies, we were unable to detect any differences in *Olfr558* mRNA expression (levels or localization) in males and females. Thus, there are likely other signals that "tell" the receptor whether it is in a male versus a female and/or which alter its downstream signaling accordingly. Moving forward, it is important to examine both a potential role for gonadal hormones to influence how ligands interact with the receptor, and whether there may be genes on the X or Y chromosome that alter some aspect of OLFR558 expression or signaling.

In conclusion, we have elucidated that an evolutionarily conserved OR is required for sex differences in blood pressure. In a mouse model, we find that *Olfr558* KO females have increased blood pressure associated with increased arterial stiffness, whereas KO males exhibit decreased DBP associated with alternations in renin and vascular reactivity. Uncovering the origin of sex differences in blood pressure regulation can help to move the field toward a more thoughtful approach to blood pressure management in both men and women.

MATERIALS AND METHODS

Ethical approval

All animal protocols and procedures were approved by the Johns Hopkins University Institutional Animal Care and Use Committee (accredited by the Association for Assessment and Accreditation of Laboratory Animal Care International).

Animals

Global *Olfr558* KO mice were generated by Ingenious Targeting Laboratory using Flexible Accelerated STOP TetO (F.A.S.T.) technology (*58*) by inserting a stop cassette before the ATG start site of *Olfr558*. *Olfr558* heterozygotes (C57BL6/N background) were bred in-house to obtain *Olfr558* WT and KO littermates. Mice were housed in individually ventilated cages with maximum of five adult mice per cage. Genotypes were confirmed by PCR of tail biopsies. All animals were given unrestricted access to food and water throughout the duration of the experiments and were maintained on Teklad 2018SX, 18% protein diet except when noted. For radio-telemetry studies, mice were housed separately in static cages placed on the telemetry receiver platform.

qPCR and RT-PCR

Mice were euthanized between 10 a.m. and 4 p.m. After euthanizing, whole tissues of interest were homogenized in TRIzol (Life Technologies) and RNA was extracted using the RNeasy Mini Kit

(QIAGEN). Isolated RNA was reverse-transcribed to cDNA using reverse transcriptase (RT-PCR) or water (mock RT-PCR). qPCR was performed using TaqMan Master Mix (Applied Biosystems) with probes for *renin* (catalog no. Mm02342887_mH, Thermo Fisher Scientific), *Akr1b7* (catalog no. Mm00477605_m1, Thermo Fisher Scientific, renin cell marker), or *Gapdh* (catalog no. Mm99999919_g1, Thermo Fisher Scientific) by cycling at 50°C for 2 min and 95°C 10 min, followed by 95°C 15 s and 60°C 1 min for 40 cycles. For *Olfr558*, SYBR green (Applied Biosystems) qPCR was performed using primers for Olfr558 forward (5′-GGGGGAAAAGACACACAGGC-3′) and reverse (5′-AAAGCCAGCCAAAACTGAACC-3′) and gapdh primers (forward: 5'-CCCTTAAGAGGGATGCTGCC-3'; reverse: 5′-ACTGTGCCGTTGAATTTGCC-3') using the cycling conditions listed above. For conventional RT-PCR, RNA was isolated from aortic and mesenteric arteries, respectively, and then reverse-transcribed to cDNA. RT-PCR was performed using the *Olfr558* primers listed above and cycling at 95°C for 5 min, followed by 94°C for 30 s, 56°C for 30 s, and 72°C for 60 s for 35 cycles, and then 72°C for 10 min. RT-PCR and mock RT-PCR were run simultaneously.

RNAScope and immunostaining

Olfr558 localization was determined using RNAScope. *Olfr558* WT and KO mice under anesthesia were perfused with phosphate-buffered saline (PBS), followed by 4% paraformaldehyde (PFA) (catalog no. 15714-S, Electron Microscopy Sciences) between 10 a.m. and 4 p.m. Tissues including the kidney, heart, BAT, skeletal muscle, testes, and ovaries were harvested; fixed in 4% PFA at 4°C overnight; and then immersed in 30% sucrose. For OE, the head (with fur, skin, and lower jaw removed) was fixed in 4% PFA at 4°C overnight and then transferred to PBS overnight. The head was immersed in EDTA solution (120 g of EDTA in 900 ml of H_2O with pH = 7.3) at 4°C for 1 week and then dehydrated with 30% sucrose (30 g of sucrose in 100 ml of PBS), 50% optimal cutting temperature compound (OCT)/50% sucrose, and lastly 100% OCT for 48 hours, 20 to 30 min, and 20 to 30 min, respectively.

For all tissues, the tissue was then frozen in OCT and cryo-sections (10 μm) were generated. RNAScope was then performed. For RNAScope, cryo-sections (10 μm) were permeabilized, retrieved, and hybridized with Mm-*Olfr558* probe (catalog no. 316131, ACDBio), followed by AMP (RNAScope@ Multiplex FL v2 AMP, ACDBio) hybridization and HRP-C1 (catalog no. 323104, ACDBio) signal development. For double-staining with antibodies (markers of cell types), sections were then blocked with superblock and incubated with rabbit anti–α-SMA (catalog no. ab5694, Abcam) or rabbit anti-renin (a generous gift from T. Inagami, Vanderbilt) antibody overnight at 4°C. Sections were then washed and incubated with Alexa Fluor 488 goat anti-rabbit secondary antibody followed by Hoechst staining. Sections were imaged using a confocal microscope (Zeiss LSM 700). For renin-glomeruli association, glomeruli were identified by Hoechst staining and then scored (+/−) for adjacent renin signal. Approximately 90% glomeruli in each section were scored. Images were taken using a fluorescence microscope (Keyence BZ-X710). For renin antibody and *Olfr558* probe double staining, quantification was performed on cells adjacent to a glomerulus that stained for *Olfr558*, renin, or both.

Olfr558 and *Olfr78* probe double staining was examined using RNAScope. Briefly, kidney or heart sections were hybridized with Mm-*Olfr558* (C1) and Mm-*Olfr78* (catalog no. 436601-C2, ACDBio) probes, and then signal was developed using HRP-C1 for Mm-Olfr558 and subsequently developed using HRP-C2 (catalog no. 323105, ACDBio) for Mm-*Olfr78*. In separate experiments, kidney sections were hybridized with Mm-Col1a2 (Col1a2, catalog no. 585461, ACDBio) and Mm-*Olfr558* (catalog no. 316131-C2, ACDBio) probes, and the signal was developed using HRP-C1 for Mm-*Col1a2* and HRP-C2 for Mm-*Olfr558*. Images were obtained by a confocal microscope (Zeiss LSM 700).

Radio-telemetry

Male and female *Olfr558* WT and KO mice (3 to 4 months old) were implanted with radio-telemetry devices (PA-C10, Data Science International) as previously described (*59*, *60*). Radio-telemetry catheters were inserted into the aorta from left carotid artery, and the body of transmitter was placed subcutaneously in the abdomen. The procedure was performed under the mixture of 1.5% isoflurane and 2% O_2. After 10 to 14 days of recovery from surgery, when the surgery site was healing well and body weight was stable, the waveform was then examined to ensure correct placement of the device catheter. If placement was incorrect, then the telemetry data from that animal were excluded from analysis. The transmitter implantation success rate was ~80 to 90%. Blood pressure was measured every 30 min with a duration of 10 s for a total of 5 days after recovery. The light/dark cycle was 7 a.m. to 9 p.m. and 9 p.m. to 7 a.m., respectively.

Wire myography

Active properties of the vessels in response to vasoconstrictors and vasodilators were examined by wire myography in both the aorta and mesenteric artery as reported (*61*). Briefly, the thoracic aorta was cut into 2-mm rings after carefully removing connective tissues. Each aortic ring was placed into Krebs buffer (containing 118 mM NaCl, 4.7 mM KCl, 2.5 mM $CaCl_2$, 1.1 mM KH_2PO_4, 25 mM $NaHCO_3$, 1.2 mM $MgSO_4$, and 11 mM glucose) and then mounted to a myograph chamber (Danish Myo Technology) and continuously bubbled with 95% O_2 and 5% CO_2 at 37°C. The rings were stretched to a final tension of 550 mg in 100-mg force increments. The second and third order mesenteric arteries were dissected and cut into 2-mm in Hepes-Tyrode solution [containing 137 mM NaCl, 2.7 mM KCl, 1.8 mM $CaCl_2$, 1 mM $MgCl_2$•$6H_2O$, 5.6 mM D-glucose, and 10 mM Hepes (pH 7.3 to 7.4)] as previously reported (*62*). Two wires were inserted into the lumen of the mesenteric artery in Hepes-Tyrode solution in a petri dish, and the vessel segments were mounted on the wire myograph chamber. All mounted vessels were submerged in Krebs buffer. The mesenteric artery was stretched to a final tension of 500 mg in 100-mg force increments. KCl (60 mM for aorta and 100 mM for mesentery) was added to determine vessel viability and obtain the maximal contractility. PE-induced vasoconstriction was studied using increasing doses of PE (10^{-9} to 10^{-5} M). Endothelial-mediated vasorelaxation was then evaluated using increasing doses of ACh (10^{-9} to 10^{-5} M) after PE preconstriction. Notably, indomentacin (3 μM; a cyclooxygenase-2 inhibitor) was added just before ACh dose response to exclude the COX pathway and, instead, focus on nitric oxide-mediated vasorelaxation. Last, endothelial-independent vasorelaxation was measured by increasing doses of SNP (10^{-9} to 10^{-5} M) in vessels preconstricted with PE.

Pulse wave velocity

PWV was measured noninvasively using a high-frequency and high-resolution Doppler spectrum analyzer, as previously reported (*61*). Briefly, *Olfr558* WT and KO females (10 weeks old) were placed supine on a 37°C plate anesthetized with 1.5% isoflurane and

2% O_2. The aortic pulse wave at the thorax and abdomen were separately recorded at a distance of ~3 cm using a 10-MHz probe, simultaneously with electrocardiograph recording. The time for the pulse wave transit from the thoracic to the abdominal aorta was measured using the electrocardiograph as a fixed point. Subsequently, PWV was calculated as the separation distance divided by the pulse transit time between the two points.

Tensile testing

The mechanical properties of intact and decellularized aortic rings were measured by tensile testing, as previously reported (*63*). Briefly, the thoracic aorta from 10-week-old *Olfr558* WT and KO females were harvested and cut into 2-mm rings. Two intact and two decellularized rings from each animal were tested. Vessel dimensions (lumen diameter, wall thickness, and length) were calculated by the transverse and longitudinal images of aortic rings obtained using a light microscope. Each vessel was then mounted on an electromechanical puller (DMT). After calibration, the pins were moved apart using an electromotor, and displacement and force applied by the vessel wall on the pin were continuously recorded. To calculate engineering stress (S), force (F) was normalized to the initial stress-free area of the specimen ($S = F/2t \times L$, where t = thickness and L = length of the aortic ring). Engineering strain (λ) was calculated as the ratio of displacement to the initial stress-free diameter. The stress-strain relationship was represented by the equation $S = \alpha \exp.(\beta\,\lambda)$, where α and β are constants. α and β were determined by nonlinear regression for each sample and used to generate stress-strain curves by treating the x axis as a continuous variable. Incremental elastic modulus (E_{inc}) was calculated as the slope of the stress-strain curve at a strain of 0.5 and 1.8.

Other in vivo studies

Whole blood samples were collected from the superficial temporal vein of 3-month-old *Olfr558* WT and KO mice and were analyzed by an iStat Chem8+ cartridge (Abbott). GFR was measured in conscious and unrestrained mice using transcutaneous measurement of fluorescein isothiocyanate (FITC)–sinistrin (MediBeacon) as previously reported (*32, 64*). Briefly, a small area on the back of the mouse was shaved and depilated with Nair under anesthesia with a mixture of 1.5% isoflurane and 2% O_2. A GFR device (MediBeacon), which measures transcutaneous fluorescence, was attached to the hairless region of the back and secured with surgical tape. A 7 mg/100 g body weight of FITC-sinistrin was retro-orbitally injected into the mouse who was then placed back into the cage with free access to water and food for 1.5 hours, after which the device was removed and data were analyzed using the MediBeacon software. Mice body weight, kidney weight/body weight (KW/BW), and heart weight/body weight (HW/BW) were measured. All in vivo data were collected from both *Olfr558* WT and KO males and females. The "*n*" for each study is noted in figure legends.

Plasma renin activity

Plasma renin activity was measured in 3-month-old *Olfr558* WT and KO mice with a modified angiotensin I measurement kit (S-1188, Peninsula Laboratories). Plasma was collected from male and female *Olfr558* WT and KO mice treated with 0.49% NaCl diet (catalog no. TD.96208 modified with orange color, Envigo). From males, we also collected plasma from mice given Teklad diet (Teklad 2018SX, 18% protein). Plasma was diluted 15-fold and then incubated with excess porcine angiotensinogen (SCP0021, Sigma-Aldrich) for 20 min at 37°C in a buffer containing 50 mM sodium acetate (pH 6.5), 10 mM 4-(2-aminoethyl) benzenesulfony fluoride hydrochloride (Sigma-Aldrich), 10 mM EDTA (pH 8.0), 1 μM porcine angiotensinogen, and 10 mM 8-hydroxyquinoline (Sigma-Aldrich). After incubation, the sample was analyzed according to the provided protocol. Plasma renin activity was assayed by competitive binding of angiotensin I antibody.

16*S* rRNA microbiome analysis

Fecal pellets (one to three for each sample) were collected from 8-week-old *Olfr558* WT and KO males and females. Fecal DNA was isolated using the Fast Stool Isolation Kit (catalog no. 51604, QIAGEN). As previously reported (*65*), the 16*S* rRNA V3 through V4 region was amplified using primers 319F (CTCCTACGGGAGGCAGCAGT) and 806R (GGACTACHVGGGTWTCTAAT). Sequencing was performed by the Johns Hopkins Transcriptomics and Deep Sequencing Core and analyzed by Resphera Biosciences as previously (*65*). Differential abundance analysis of α-diversity analyzed differences between groups (nonparametric difference test, Mann-Whitney *U* test, and *t* test). Multiple hypothesis testing was corrected using the false discovery rate. Generalized linear modeling was performed using R. 16*S* data have been deposited to the National Center for Biotechnology Information (www.ncbi.nlm.nih.gov/Traces/study/?acc=PRJNA902003&o=acc_s%3Aa).

Human genetic analysis

A previous GWAS (*45*) identified *OR51E1* as a locus significantly associated with DBP. Here, we performed new genetic association analyses of DBP within the UKB cohort to conduct more detailed stratified analyses of this published variant and also to analyze a new rare variant of interest. We used the same dataset that was used for the previous GWAS (table S2), as described (*45*). All UKB individuals analyzed are of European ancestry. To perform simple linear regression analyses, we excluded first and second degree relatives, leaving a total of $n = 423{,}657$ individuals for analysis. Linear regression analyses testing the association of the genetic variant with DBP were adjusted for the following covariates: sex, age, age^2, body mass index, genotyping chip subset of UKB, and top 10 principal components of ancestry. Sex-stratified analyses were performed using two separate subgroups to compare males versus females. In addition, an analysis was performed on all individuals with a sex-interaction term to identify any sex-specific effects. Last, given the changes in blood pressure that occur with aging (particularly in women), we also performed age-stratified analyses in women (<50 versus >50 years) and in men (<50 versus >50 years) and a corresponding age-interaction analysis. Within each analyzed subgroup, we calculated the mean DBP measurement for creation of plots. We performed analyses for two variants: (i) the common missense variant, rs17224476 [chr11:4673788, National Center for Biotechnology Information (NCBI) build 37], previously identified by Evangelou *et al.* (*45*) as the lead variant at the *OR51E1* locus achieving the most significant association for DBP and (ii) a rare missense variant, rs202113356, which we previously published to alter OR51E1 function (chr11:4673788, NCBI build 37) (*34*). This rare variant had not been analyzed previously by Evangelou *et al.*, as the published GWAS only included common variants. As rs202113356 is a rare variant, there were no individuals in UKB with two copies of the minor allele A. Thus, for consistency, all of our statistical analyses for both variants are performed according to a binary

genotype model comparing noncarriers (GG) versus carriers of the minor allele (AG/AA). The common variant (rs17224476) is directly genotyped within the UKB data, whereas the rare variant (rs202113356) is extracted from the imputed genetic data, with high imputation quality Rsq = 0.8. For analysis by genotype groups, the genetic data were converted to hard-call genotype format using PLINK software, yielding $N = 58$ individuals with missing data for the imputed rare variant if their imputation certainty did not reach the hard-call threshold in PLINK.

Cloning and immunofluorescence

OR51E1 has been previously cloned with Lucy-Flag-Rho tags at the N terminus in the pME18S vector (*32*). In addition, we previously reported that Lucy and Rho tags promote surface expression of ORs (*66*). Thus, we used the Lucy-Flag-Rho tags for *OR51E1* variants—rs202113356 (OR51E1 A156T) and rs17224476 (OR51E1 S10N). The OR51E1 A156T mutant was generated as part of a previous study (*34*); the S10N mutant was generated for this study via PCR and sequenced to confirm. To examine OR expression and surface trafficking, human embryonic kidney (HEK) 293 T cells were seeded onto poly-L-lysine–coated coverslips and transfected with OR constructs with receptor transporting protein 1S (RTP1S) and/or olfactory G protein (Golf), as we previously reported (*34*). Cell surface staining was done in live cells blocked with diluted superblock (1:4 dilution in PBS with 1 mM $MgCl_2$ and 0.1 mM $CaCl_2$, Thermo Fisher Scientific) at 4°C for 0.5 hours and incubated with rabbit polyclonal anti-flag antibody (catalog no. F7435, MilliporeSigma) at 1:100 diluted superblock at 4°C for 1 hour. The flag tag on these constructs is on the N terminus, and thus can only be labeled in live cells if the OR reaches the cell surface. Cells were then washed, fixed with 4% PFA, permeabilized with 0.3% Triton X-100, and blocked with diluted superblock for 1 hour at room temperature. Total expression staining was assayed in fixed, permeabilized cells by staining with mouse monoclonal anti-flag antibody (M2, catalog no. F1802, MilliporeSigma) at 1:100 in diluted superblock at 4°C overnight. All surface and total staining cells were incubated with secondary antibody at 1:1000 in diluted superblock with Hoechst 33342 (catalog no. LSH3570, Invitrogen Molecular Probes) at 1:2500 dilution in the dark for 1 hour at room temperature. Last, cells were washed and mounted using VECTASHIELD Hard Set mounting medium (H-1400, Vector Laboratories). Images were taken using a confocal microscope (Zeiss LSM 700). Images were quantified manually by ImageJ by quantifying the signal per cell (quantified in every positive cell within the field of view; values for cells within the same field of view were averaged). Thus, each "*n*" represents the average of values for a given field of view.

Real-time cAMP assay

HEK 293T cells were seeded into a poly-L-lysine–coated black 96-well plate with a clear bottom and incubated overnight. Cells were transfected with OR51E1 or OR51E1 variants with RTP1S and/or Golf. After 4-hour transfection, the cADDis cAMP sensor (BacMan baculovirus, catalog no. U0205G, Montana Molecular) was transduced into the cells. The cAMP fluorescence was measured 24 hours after the sensor transfection at excitation of 490-nm and emission of 525-nm wavelengths. Real-time cAMP production was measured before and every minute after stimulus for a total 10 min. The stimulus was present during the 10-min sampling period. Stimuli were sodium butyrate (catalog no. 303410, MilliporeSigma), IVA (catalog no. 129542, MilliporeSigma), VA (catalog no. 240370, MilliporeSigma), 3-MVA (3-MVA, catalog no. 222453, MilliporeSigma), 4-MVA (catalog no. 277827, MilliporeSigma), and CCA (catalog no. C95609, MilliporeSigma).

ELISA

Total protein expression of the OR51E1 constructs in HEK 293T cells was measured by enzyme-linked immunosorbent assay (ELISA), as previously reported (*34, 66*). Cells were grown in a poly-L-lysine 96-well-plate (black plate with clear bottoms) and transfected with OR51E1 or OR51E1 variants with RTP1S and with or without Golf. After 24-hour transfection, cells were fixed, permeabilized, and incubated with mouse monoclonal anti-flag antibody (M2, catalog no. F1802, MilliporeSigma) at 1:100 dilution and detected with anti-mouse horseradish peroxidase (HRP)–conjugated secondary antibody (catalog no. 115-035-146, the Jackson Laboratory) at 1:8000 dilution. HRP levels were measured with 1-Step Ultra TMB (3,3′,5,5′-tetramethylbenzidine; catalog no. 34028, Thermo Fisher Scientific) at excitation of 450 nm.

RNA-seq data

We downloaded *OR51E1* expression in kidney cell types from the Kidney Precision Medicine Project (https://atlas.kpmp.org/explorer/dataviz) and *OR51E1* expression in other organs from the Human Protein Atlas (www.proteinatlas.org/ENSG00000180785-OR51E1/single+cell+type) including the heart muscle (https://v22.proteinatlas.org/ENSG00000180785-OR51E1/single+cell+type/heart+muscle), vascular (https://v22.proteinatlas.org/ENSG00000180785-OR51E1/single+cell+type/Vascular), adipose (https://v22.proteinatlas.org/ENSG00000180785-OR51E1/single+cell+type/adipose+tissue), skeletal muscle (https://v22.proteinatlas.org/ENSG00000180785-OR51E1/single+cell+type/skeletal+muscle), and liver (https://v22.proteinatlas.org/ENSG00000180785-OR51E1/single+cell+type/liver). These data were downloaded in March 2023.

Ethics statement

The UKB study has approval from the North West Multi-Centre Research Ethics Committee. Any participants from UKB who withdrew consent were removed from our analysis.

Statistical analysis

Data are presented as means ± SEM. Sample size (*n*) is indicated for each reported value. Statistical significance was determined by *t* test or analysis of variance (ANOVA) with Tukey's post hoc analysis for multiple groups ($P < 0.05$). For human genetic data analysis, linear regression analyses were performed using R statistical software (https://www.r-project.org/).

Supplementary Materials

This PDF file includes:

Figs. S1 to S17
Tables S1 to S3
Legend for table S4

Other Supplementary Material for this manuscript includes the following:

Table S4

REFERENCES AND NOTES

1. G. Barsha, K. M. Denton, K. M. Mirabito Colafella, Sex- and age-related differences in arterial pressure and albuminuria in mice. *Biol. Sex Differ.* **7**, 57 (2016).
2. A. T. Robinson, M. M. Wenner, N. Charkoudian, Differential influences of dietary sodium on blood pressure regulation based on race and sex. *Auton. Neurosci.* **236**, 102873 (2021).

3. M. Sahinoz, F. Elijovich, L. A. Ertuglu, J. Ishimwe, A. Pitzer, M. Saleem, N. Mwesigwa, T. R. Kleyman, C. L. Laffer, A. Kirabo, Salt sensitivity of blood pressure in blacks and women: A role of inflammation, oxidative stress, and epithelial Na^+ channel. *Antioxid. Redox Signal.* **35**, 1477–1493 (2021).
4. J. F. Reckelhoff, Androgens and blood pressure control: Sex differences and mechanisms. *Mayo Clin. Proc.* **94**, 536–543 (2019).
5. J. F. Reckelhoff, Sex differences in regulation of blood pressure. *Adv. Exp. Med. Biol.* **1065**, 139–151 (2018).
6. N. Wiinberg, A. Hoegholm, H. R. Christensen, L. E. Bang, K. L. Mikkelsen, P. E. Nielsen, T. L. Svendsen, J. P. Kampmann, N. H. Madsen, M. W. Bentzon, 24-h ambulatory blood pressure in 352 normal Danish subjects, related to age and gender. *Am. J. Hypertens.* **8**, 978–986 (1995).
7. J. F. Reckelhoff, Gender differences in the regulation of blood pressure. *Hypertension* **37**, 1199–1208 (2001).
8. A. K. Wills, D. A. Lawlor, F. E. Matthews, A. A. Sayer, E. Bakra, Y. Ben-Shlomo, M. Benzeval, E. Brunner, R. Cooper, M. Kivimaki, D. Kuh, G. Muniz-Terrera, R. Hardy, Life course trajectories of systolic blood pressure using longitudinal data from eight UK cohorts. *PLOS Med.* **8**, e1000440 (2011).
9. H. Ji, A. Kim, J. E. Ebinger, T. J. Niiranen, B. L. Claggett, C. N. Bairey Merz, S. Cheng, Sex differences in blood pressure trajectories over the life course. *JAMA Cardiol.* **5**, 19–26 (2020).
10. H. Ji, T. J. Niiranen, F. Rader, M. Henglin, A. Kim, J. E. Ebinger, B. Claggett, C. N. B. Merz, S. Cheng, Sex differences in blood pressure associations with cardiovascular outcomes. *Circulation* **143**, 761–763 (2021).
11. J. Staessen, C. J. Bulpitt, R. Fagard, G. Mancia, E. T. O'Brien, L. Thijs, G. Vyncke, A. Amery, Reference values for the ambulatory blood pressure and the blood pressure measured at home: A population study. *J. Hum. Hypertens.* **5**, 355–361 (1991).
12. J. Staessen, C. J. Bulpitt, R. Fagard, G. Mancia, E. T. O'Brien, L. Thijs, G. Vyncke, A. Amery, Reference values for ambulatory blood pressure: A population study. *J. Hypertens. Suppl.* **9**, S320–S321 (1991).
13. H. Nakatsuka, Y. Imai, K. Abe, K. Nagai, M. Ikeda, H. Satoh, S. Sasaki, N. Minami, M. Munakata, H. Sakuma, J. Hashimoto, H. Sekino, K. Imai, K. Yoshinaga, Population study of ambulatory blood pressure in a rural community in northern Japan. *Tohoku J. Exp. Med.* **163**, 119–127 (1991).
14. C. Maric-Bilkan, M. B. Manigrasso, Sex differences in hypertension: Contribution of the renin-angiotensin system. *Gend. Med.* **9**, 287–291 (2012).
15. J. M. Shelley, A. Green, A. M. Smith, E. Dudley, L. Dennerstein, J. Hopper, H. Burger, Relationship of endogenous sex hormones to lipids and blood pressure in mid-aged women. *Ann. Epidemiol.* **8**, 39–45 (1998).
16. C. M. Masi, L. C. Hawkley, J. D. Berry, J. T. Cacioppo, Estrogen metabolites and systolic blood pressure in a population-based sample of postmenopausal women. *J. Clin. Endocrinol. Metab.* **91**, 1015–1020 (2006).
17. Y. A. Shakir, G. Samsioe, P. Nyberg, J. Lidfeldt, C. Nerbrand, Cardiovascular risk factors in middle-aged women and the association with use of hormone therapy: Results from a population-based study of Swedish women. The Women's Health in the Lund Area (WHILA) Study. *Climacteric* **7**, 274–283 (2004).
18. T. Vikan, H. Schirmer, I. Njolstad, J. Svartberg, Endogenous sex hormones and the prospective association with cardiovascular disease and mortality in men: The Tromsø Study. *Eur. J. Endocrinol.* **161**, 435–442 (2009).
19. K. T. Khaw, M. Dowsett, E. Folkerd, S. Bingham, N. Wareham, R. Luben, A. Welch, N. Day, Endogenous testosterone and mortality due to all causes, cardiovascular disease, and cancer in men: European prospective investigation into cancer in Norfolk (EPIC-Norfolk) prospective population study. *Circulation* **116**, 2694–2701 (2007).
20. G. A. Laughlin, E. Barrett-Connor, J. Bergstrom, Low serum testosterone and mortality in older men. *J. Clin. Endocrinol. Metab.* **93**, 68–75 (2008).
21. H. Ji, W. Zheng, X. Wu, J. Liu, C. M. Ecelbarger, R. Watkins, A. P. Arnold, K. Sandberg, Sex chromosome effects unmasked in angiotensin II-induced hypertension. *Hypertension* **55**, 1275–1282 (2010).
22. L. Buck, R. Axel, A novel multigene family may encode odorant receptors: A molecular-basis for odor recognition. *Cell* **65**, 175–187 (1991).
23. M. Spehr, G. Gisselmann, A. Poplawski, J. A. Riffell, C. H. Wetzel, R. K. Zimmer, H. Hatt, Identification of a testicular odorant receptor mediating human sperm chemotaxis. *Science* **299**, 2054–2058 (2003).
24. A. Pronin, K. Levay, D. Velmeshev, M. Faghihi, V. I. Shestopalov, V. Z. Slepak, Expression of olfactory signaling genes in the eye. *PLOS ONE* **9**, e96435 (2014).
25. J. L. Pluznick, R. J. Protzko, H. Gevorgyan, Z. Peterlin, A. Sipos, J. Han, I. Brunet, L.-X. Wan, F. Rey, T. Wang, S. J. Firestein, M. Yanagisawa, J. I. Gordon, A. Eichmann, J. Peti-Peterdi, M. J. Caplan, Olfactory receptor responding to gut microbiota-derived signals plays a role in renin secretion and blood pressure regulation. *Proc. Natl. Acad. Sci. U.S.A.* **110**, 4410–4415 (2013).
26. Y. Niimura, A. Matsui, K. Touhara, Extreme expansion of the olfactory receptor gene repertoire in African elephants and evolutionary dynamics of orthologous gene groups in 13 placental mammals. *Genome Res.* **25**, 926–926 (2015).
27. D. Priori, M. Colombo, P. Clavenzani, A. J. M. Jansman, J. P. Lalles, P. Trevisi, P. Bosi, The olfactory receptor OR51E1 is present along the gastrointestinal tract of pigs, co-localizes with enteroendocrine cells and is modulated by intestinal microbiota. *PLOS ONE* **10**, e0129501 (2015).
28. K. A. Adipietro, J. D. Mainland, H. Matsunami, Functional evolution of mammalian odorant receptors. *PLOS Genet.* **8**, e1002821 (2012).
29. A. Pronin, V. Slepak, Ectopically expressed olfactory receptors OR51E1 and OR51E2 suppress proliferation and promote cell death in a prostate cancer cell line. *J. Biol. Chem.* **296**, 100475 (2021).
30. R. C. Jimenez, N. Casajuana-Martin, A. Garcia-Recio, L. Alcantara, L. Pardo, M. Campillo, A. Gonzalez, The mutational landscape of human olfactory G protein-coupled receptors. *BMC Biol.* **19**, 21 (2021).
31. C. Flegel, S. Manteniotis, S. Osthold, H. Hatt, G. Gisselmann, Expression profile of ectopic olfactory receptors determined by deep sequencing. *PLOS ONE* **8**, e55368 (2013).
32. V. L. Halperin Kuhns, J. L. Pluznick, Novel differences in renal gene expression in a diet-induced obesity model. *Am. J. Physiol. Renal Physiol.* **314**, F517–F530 (2018).
33. V. L. Halperin Kuhns, J. Sanchez, D. C. Sarver, Z. Khalil, P. Rajkumar, K. A. Marr, J. L. Pluznick, Characterizing novel olfactory receptors expressed in the murine renal cortex. *Am. J. Physiol. Renal Physiol.* **317**, F172–F186 (2019).
34. J. Xu, J. L. Pluznick, Key amino acids alter activity and trafficking of a well-conserved olfactory receptor. *Am. J. Physiol. Cell Physiol.* **322**, C1279–C1288 (2022).
35. H. Saito, Q. Chi, H. Zhuang, H. Matsunami, J. D. Mainland, Odor coding by a Mammalian receptor repertoire. *Sci. Signal.* **2**, ra9 (2009).
36. Y. Fujita, T. Takahashi, A. Suzuki, K. Kawashima, F. Nara, R. Koishi, Deorphanization of Dresden G protein-coupled receptor for an odorant receptor. *J. Recept. Signal Transduct. Res.* **27**, 323–334 (2007).
37. N. Jovancevic, A. Dendorfer, M. Matzkies, M. Kovarova, J. C. Heckmann, M. Osterloh, M. Boehm, L. Weber, F. Nguemo, J. Semmler, J. Hescheler, H. Milting, E. Schleicher, L. Gelis, H. Hatt, Medium-chain fatty acids modulate myocardial function via a cardiac odorant receptor. *Basic Res. Cardiol.* **112**, 13 (2017).
38. B. Kalbe, M. Schlimm, S. Wojcik, S. Philippou, D. Massberg, F. Jansen, P. Scholz, H. Luebbert, B. Ubrig, S. Osterloh, H. Hatt, Olfactory signaling components and olfactory receptors are expressed in tubule cells of the human kidney. *Arch. Biochem. Biophys.* **610**, 8–15 (2016).
39. E. J. Macarak, P. J. Wermuth, J. Rosenbloom, J. Uitto, Keloid disorder: Fibroblast differentiation and gene expression profile in fibrotic skin diseases. *Exp. Dermatol.* **30**, 132–145 (2021).
40. I. M. H. Li, A. L. Horwell, G. Chu, B. de Crombrugghe, G. Bou-Gharios, Characterization of mesenchymal-fibroblast cells using the *Col1a2* promoter/enhancer. *Methods Mol. Biol.* **1627**, 139–161 (2017).
41. S. Serizawa, K. Miyamichi, H. Sakano, One neuron-one receptor rule in the mouse olfactory system. *Trends Genet.* **20**, 648–653 (2004).
42. M. Karlsson, C. Zhang, L. R. Mear, W. Zhong, A. Digre, B. Katona, E. Sjostedt, L. Butler, J. Odeberg, P. Dusart, F. Edfors, P. Oksvold, K. von Feilitzen, M. Zwahlen, M. Arif, O. Altay, X. Y. Li, M. Ozcan, A. Mardonoglu, L. Fagerberg, J. Mulder, Y. L. Luo, F. Ponten, M. Uhlen, C. Lindskog, A single-cell type transcriptomics map of human tissues. *Sci. Adv.* **7**, eabh2169 (2021).
43. B. B. Lake, R. Menon, S. Winfree, Q. Hu, R. M. Ferreira, K. Kalhor, D. Barwinska, E. A. Otto, M. Ferkowicz, D. Diep, N. Plongthongkum, A. Knoten, S. Urata, L. H. Mariani, A. S. Naik, S. Eddy, B. Zhang, Y. Wu, D. Salamon, J. C. Williams, X. Wang, K. S. Balderrama, P. J. Hoover, E. Murray, J. L. Marshall, T. Noel, A. Vijayan, A. Hartman, F. Chen, S. S. Waikar, S. E. Rosas, F. P. Wilson, P. M. Palevsky, K. Kiryluk, J. R. Sedor, R. D. Toto, C. R. Parikh, E. H. Kim, R. Satija, A. Greka, E. Z. Macosko, P. V. Kharchenko, J. P. Gaut, J. B. Hodgin; KPMP Consortium, M. T. Eadon, P. C. Dagher, T. M. El-Achkar, K. Zhang, M. Kretzler, S. Jain, An atlas of healthy and injured cell states and niches in the human kidney. BioRxiv 454201 [Preprint]. 29 July 2021.
44. R. M. Castellanos-Rivera, E. S. Pentz, E. Lin, K. W. Gross, S. Medrano, J. Yu, M. L. Sequeira-Lopez, R. A. Gomez, Recombination signal binding protein for Ig-κJ region regulates juxtaglomerular cell phenotype by activating the myo-endocrine program and suppressing ectopic gene expression. *J. Am. Soc. Nephrol.* **26**, 67–80 (2015).
45. E. Evangelou, H. R. Warren, D. Mosen-Ansorena, B. Mifsud, R. Pazoki, H. Gao, G. Ntritsos, N. Dimou, C. P. Cabrera, I. Karaman, F. L. Ng, M. Evangelou, K. Witkowska, E. Tzanis, J. N. Hellwege, A. Giri, D. R. V. Edwards, Y. V. Sun, K. Cho, J. M. Gaziano, P. W. F. Wilson, P. S. Tsao, C. P. Kovesdy, T. Esko, R. Magi, L. Milani, P. Almgren, T. Boutin, S. Debette, J. Ding, F. Giulianini, E. G. Holliday, A. U. Jackson, R. Li-Gao, W. Y. Lin, J. A. Luan, M. Mangino, C. Oldmeadow, B. P. Prins, Y. Qian, M. Sargurupremraj, N. Shah, P. Surendran, S. Theriault, N. Verweij, S. M. Willems, J. H. Zhao, P. Amouyel, J. Connell, R. de Mutsert, A. S. F. Doney, M. Farrall, C. Menni, A. D. Morris, R. Noordam, G. Pare, N. R. Poulter, D. C. Shields, A. Stanton, S. Thom, G. Abecasis, N. Amin, D. E. Arking, K. L. Ayers, C. M. Barbieri, C. Batini, J. C. Bis, T. Blake, M. Bochud, M. Boehnke, E. Boerwinkle, D. I. Boomsma, E. P. Bottinger, P. S. Braund, M. Brumat, A. Campbell, H. Campbell, A. Chakravarti, J. C. Chambers, G. Chauhan, M. Ciullo, M. Cocca, F. Collins, H. J. Cordell, G. Davies, M. H. de Borst,

E. J. de Geus, I. J. Deary, J. Deelen, M. F. Del Greco, C. Y. Demirkale, M. Dorr, G. B. Ehret, R. Elosua, S. Enroth, A. M. Erzurumluoglu, T. Ferreira, M. Franberg, O. H. Franco, I. Gandin, P. Gasparini, V. Giedraitis, C. Gieger, G. Girotto, A. Goel, A. J. Gow, V. Gudnason, X. Q. Guo, U. Gyllensten, A. Hamsten, T. B. Harris, S. E. Harris, C. A. Hartman, A. S. Havulinna, A. A. Hicks, E. Hofer, A. Hofman, J. J. Hottenga, J. E. Huffman, S. J. Hwang, E. Ingelsson, A. James, R. Jansen, M. R. Jarvelin, R. Joehanes, A. Johansson, A. D. Johnson, P. K. Joshi, P. Jousilahti, J. W. Jukema, A. Jula, M. Kahonen, S. Kathiresan, B. D. Keavney, K. T. Khaw, P. Knekt, J. Knight, I. Kolcic, J. S. Kooner, S. Koskinen, K. Kristiansson, Z. Kutalik, M. Laan, M. Larson, L. J. Launer, B. Lehne, T. Lehtimaki, D. C. M. Liewald, L. Lin, L. Lind, C. M. Lindgren, Y. M. Liu, R. J. F. Loos, L. M. Lopez, Y. C. Lu, L. P. Lyytikainen, A. Mahajan, C. Mamasoula, J. Marrugat, J. Marten, Y. Milaneschi, A. Morgan, A. P. Morris, A. C. Morrison, P. J. Munson, M. A. Nalls, P. Nandakumar, C. P. Nelson, T. Niiranen, I. M. Nolte, T. Nutile, A. J. Oldehinkel, B. A. Oostra, P. F. O'Reilly, E. Org, S. Padmanabhan, W. Palmas, A. Palotie, A. Pattie, B. W. J. H. Penninx, M. Perola, A. Peters, O. Polasek, P. P. Pramstaller, Q. T. Nguyen, O. T. Raitakari, M. Ren, R. Rettig, K. Rice, P. M. Ridker, J. S. Ried, H. Riese, S. Ripatti, A. Robino, L. M. Rose, J. I. Rotter, I. Rudan, D. Ruggiero, Y. Saba, C. F. Sala, V. Salomaa, N. J. Samani, A. P. Sarin, R. Schmidt, H. Schmidt, N. Shrine, D. Siscovick, A. V. Smith, H. Snieder, S. Sober, R. Sorice, J. M. Starr, D. J. Stott, D. P. Strachan, R. J. Strawbridge, J. Sundstrom, M. A. Swertz, K. D. Taylor, A. Teumer, M. D. Tobin, M. Tomaszewski, D. Toniolo, M. Traglia, S. Trompet, J. Tuomilehto, C. Tzourio, A. G. Uitterlinden, A. Vaez, P. J. van der Most, C. M. van Duijn, A. C. Vergnaud, G. C. Verwoert, V. Vitart, U. Volker, P. Vollenweider, D. Vuckovic, H. Watkins, S. H. Wild, G. Willemsen, J. F. Wilson, A. F. Wright, J. Yao, T. Zemunik, W. H. Zhang, J. R. Attia, A. S. Butterworth, D. I. Chasman, D. Conen, F. Cucca, J. Danesh, C. Hayward, J. M. M. Howson, M. Laakso, E. G. Lakatta, C. Langenberg, O. Melander, D. O. Mook-Kanamori, C. N. A. Palmer, L. Risch, R. A. Scott, R. J. Scott, P. Sever, T. D. Spector, P. van der Harst, N. J. Wareham, E. Zeggini, D. Levy, P. B. Munroe, C. Newton-Cheh, M. J. Brown, A. Metspalu, A. M. Hung, C. J. O'Donnell, T. L. Edwards, Million Veteran Program, B. M. Psaty, I. Tzoulaki, M. R. Barnes, L. V. Wain, P. Elliott, M. J. Caulfield, Publisher Correction: Genetic analysis of over 1 million people identifies 535 new loci associated with blood pressure traits. *Nat. Genet.* **50**, 1755 (2018).

46. J. W. Lee, C. L. Chou, M. A. Knepper, Deep sequencing in microdissected renal tubules identifies nephron segment-specific transcriptomes. *J. Am. Soc. Nephrol.* **26**, 2669–2677 (2015).
47. E. W. Brunskill, M. L. S. Sequeira-Lopez, E. S. Pentz, E. Lin, J. Yu, B. J. Aronow, S. S. Potter, R. A. Gomez, Genes that confer the identity of the renin cell. *J. Am. Soc. Nephrol.* **23**, 2213–2225 (2012).
48. A. J. Chang, F. E. Ortega, J. Riegler, D. V. M. Adison, M. A. Krasnow, Oxygen regulation of breathing through an olfactory receptor activated by lactate. *Nature* **527**, 240–244 (2015).
49. N. W. Bellono, J. R. Bayrer, D. B. Leitch, J. Castro, C. C. Zhang, T. A. O'Donnell, S. M. Brierley, H. A. Ingraham, D. Julius, Enterochromaffin cells are gut chemosensors that couple to sensory neural pathways. *Cell* **170**, 185–198.e16 (2017).
50. K. Conradi, J. Jelinek, F. Gross, Strain and sex differences in renin content of rat kidneys. *Proc. Soc. Exp. Biol. Med.* **132**, 984–986 (1969).
51. A. W. Cowley Jr., M. M. Skelton, M. T. Velasquez, Sex differences in the endocrine predictors of essential hypertension. Vasopressin Versus Renin. *Hypertension* **7**, I151–I160 (1985).
52. K. D. Pendergrass, N. T. Pirro, B. M. Westwood, C. M. Ferrario, K. B. Brosnihan, M. C. Chappell, Sex differences in circulating and renal angiotensins of hypertensive mRen(2). Lewis but not normotensive Lewis rats. *Am. J. Physiol. Heart. Circ. Physiol.* **295**, H10–H20 (2008).
53. O. Guessoum, M. Zainab, M. L. S. Sequeira-Lopez, R. A. Gomez, Proliferation does not contribute to murine models of renin cell recruitment. *Acta Physiol.* **230**, e13532 (2020).
54. I. Sakuma, M. Y. Liu, A. Sato, T. Hayashi, A. Iguchi, A. Kitabatake, Y. Hattori, Endothelium-dependent hyperpolarization and relaxation in mesenteric arteries of middle-aged rats: Influence of oestrogen. *Br. J. Pharmacol.* **135**, 48–54 (2002).
55. J. N. Stallone, Role of endothelium in sexual dimorphism in vasopressin-induced contraction of rat aorta. *Am. J. Physiol.* **265**, H2073–H2080 (1993).
56. J. K. Crews, R. A. Khalil, Gender-specific inhibition of Ca^{2+} entry mechanisms of arterial vasoconstriction by sex hormones. *Clin. Exp. Pharmacol. Physiol.* **26**, 707–715 (1999).
57. C. A. Kanashiro, R. A. Khalil, Gender-related distinctions in protein kinase C activity in rat vascular smooth muscle. *Am. J. Physiol. Cell Physiol.* **280**, C34–C45 (2001).
58. K. F. Tanaka, S. E. Ahmari, E. D. Leonardo, J. W. Richardson-Jones, E. C. Budreck, P. Scheiffele, S. Sugio, N. Inamura, K. Ikenaka, R. Hen, Flexible Accelerated STOP Tetracycline Operator-Knockin (FAST): A versatile and efficient new gene modulating system. *Biol. Psychiatry* **67**, 770–773 (2010).
59. B. G. Poll, J. Xu, S. Jun, J. Sanchez, N. A. Zaidman, X. He, L. Lester, D. E. Berkowitz, N. Paolocci, W. D. Gao, J. L. Pluznick, Acetate, a short-chain fatty acid, acutely lowers heart rate and cardiac contractility along with blood pressure. *J. Pharmacol. Exp. Ther.* **377**, 39–50 (2021).
60. B. G. Poll, J. Xu, K. Gupta, T. B. Shubitowski, J. L. Pluznick, Olfactory receptor 78 modulates renin but not baseline blood pressure. *Physiol. Rep.* **9**, e15017 (2021).
61. L. Santhanam, G. Q. Liu, S. Jandu, W. P. Su, B. P. Wodu, W. Savage, A. Poe, X. N. Liu, L. M. Alexander, X. Cao, M. Wan, Skeleton-secreted PDGF-BB mediates arterial stiffening. *J. Clin. Invest.* **131**, e147116 (2021).
62. J. Sun, G. M. Yang, T. Tao, L. S. Wei, Y. Pan, M. S. Zhu, Isometric contractility measurement of the mouse mesenteric artery using wire myography. *J. Vis. Exp.*, 58064 (2018).
63. E. Tuday, M. Nakano, K. Akiyoshi, X. Fu, A. P. Shah, A. Yamaguchi, C. Steenbergen, L. Santhanam, S. S. An, D. Berkowitz, J. M. Baraban, S. Das, Degradation of premature-miR-181b by the translin/trax RNase increases vascular smooth muscle cell stiffness. *Hypertension* **78**, 831–839 (2021).
64. B. D. Shepard, H. Koepsell, J. L. Pluznick, Renal olfactory receptor 1393 contributes to the progression of type 2 diabetes in a diet-induced obesity model. *Am. J. Physiol. Renal. Physiol.* **316**, F372–F381 (2019).
65. M. U. Cheema, J. L. Pluznick, Gut microbiota plays a central role to modulate the plasma and fecal metabolomes in response to angiotensin II. *Hypertension* **74**, 184–193 (2019).
66. B. D. Shepard, N. Natarajan, R. J. Protzko, O. W. Acres, J. L. Pluznick, A cleavable N-terminal signal peptide promotes widespread olfactory receptor surface expression in HEK293T cells. *PLOS ONE* **8**, e68758 (2013).
67. F. Wang, J. Flanagan, N. Su, L.-C. Wang, S. Bui, A. Nielson, X. Wu, H.-T. Vo, X.-J. Ma, Y. Luo, RNAscope: A novel in situ RNA analysis platform for formalin-fixed, paraffin-embedded tissues. *J. Mol. Diagn.* **14**, 22–29 (2012).

Acknowledgments: We would like to thank J. Sanchez, D. Sarver, J. Sun, S. Wu, B. Poll, P. Richard Grimm (JHU), and M. L. Sequeira-Lopez (U Virginia) for the advice and help. We also thank past and present Pluznick Laboratory members for helpful discussion, suggestions, and comments. This research has been conducted using the UKB Resource under application no. 236. **Funding:** This work was supported by R56DK107726 [National Institutes of Health National Institute of Diabetes and Digestive and Kidney Diseases (NIH NIDDK)], R21AG081683 (NIH National Institute on Aging), and American Heart Association Established Investigator Award 949866 (to J.L.P.). H.R.W. acknowledges the funding of the NIHR Cardiovascular Biomedical Centre at Barts and The London, Queen Mary University of London. **Author contributions:** J.L.P., J.X. and L.S. conceived and designed the research. J.X., R.C., H.W., and K.G. performed the experiments. J.X., R.C., and H.W. analyzed the data. J.L.P., J.X., and L.S. interpreted the data. J.X. and J.L.P. wrote the manuscript. J.L.P. and H.W. provided funding. All authors read and approved the final manuscript. **Competing interests:** The authors declare that they have no competing interests. **Data and materials availability:** All data needed to evaluate the conclusions in the paper are present in the paper and/or the Supplementary Materials.

Submitted 4 August 2023
Accepted 13 February 2024
Published 20 March 2024
10.1126/sciadv.adk1487